Manuscript prepared for Biogeosciences
with version 2014/09/16 7.15 Copernicus papers of the LaTeX class copernicus.cls.
Date: 27 July 2015

New insights into the organic carbon export in the Mediterranean Sea from 3D modeling

A. Guyennon[1], M. Baklouti[1], F. Diaz[1], J. Palmieri[2], J. Beuvier[3,4], C. Lebaupin-Brossier[4], T. Arsouze[5,6], K. Béranger[5], J.-C. Dutay[7], and T. Moutin[1]

[1]Aix Marseille Université, CNRS/INSU, Université de Toulon, IRD, Mediterranean Institute of Oceanography (MIO) UM110, 13288, Marseille, France
[2]Southampton University – National Oceanography Center (NOC), Waterfront Campus, European Way, Southampton SO14 3ZH, UK
[3]Mercator Ocean, Ramonville Saint-Agne, France
[4]CNRM-GAME, Météo-France/CNRS, Toulouse, France
[5]UME, ENSTA-ParisTech, Palaiseau, France
[6]Laboratoire de Météorologie Dynamique, École Polytechnique, Palaiseau, France
[7]LSCE/IPSL, Laboratoire des Sciences du Climat et de l'Environnement, CEA-CNRS-UVSQ, Gif-sur-Yvette, France

Correspondence to: melika.baklouti@mio.osupytheas.fr

COLOR CODE:

RED = DELETED TEXT

BLUE = NEW TEXT

BLACK = OLD TEXT

Abstract. The Mediterranean Sea is one of the most oligotrophic regions of the oceans, and nutrients have been shown to limit both phytoplankton and bacterial activities. This has direct implications on the stock of dissolved organic carbon (DOC), whose high variability has already been well-documented even if measurements are still sparse and are associated with important uncertainties. We here propose a Mediterranean basin-scale view of the export of organic carbon, under its dissolved and particulate forms. For this purpose, we have used a coupled model combining a mechanistic biogeochemical model (Eco3M-MED) and a high-resolution (eddy-resolving) hydrodynamic simulation (NEMO-MED12). This is the first basin-scale application of the biogeochemical model Eco3M-MED and is shown to reproduce the main spatial and seasonal biogeochemical characteristics of the Mediterranean Sea. Model estimations of carbon export are of the same order of magnitude as estimations from in situ observations, and their respective spatial patterns are consistent with each other. As for surface chlorophyll, nutrient concentrations, and productivity, strong differences between the Western and Eastern basins are evidenced by the model for organic carbon export, with only 39 % of organic carbon (particulate and dissolved) export taking place in the Western basin.

The major result is that except for the Alboran Sea, dissolved organic carbon (DOC) contribution to organic carbon export is higher than that of particulate (POC) in the whole basin, especially in the Eastern basin. This paper also investigates the seasonality of DOC and POC exports as well as the differences in the processes involved in DOC and POC exports in the light of intracellular quotas.

1 Introduction

The biological pump is recognized as a major component of carbon export by the ocean and plays a significant role in the carbon cycle as a whole (Siegenthaler and Sarmiento, 1993). The sinking of organic particles has long been identified as the main process involved in the biological pump, sustaining the vertical carbon and nutrient gradients in the ocean (Sarmiento and Gruber, 2006; Eppley and Peterson, 1979). Major attention has therefore been paid to the export of organic carbon under its particulate form. , as this is the end of the carbon pathway.

The improvement of the characterization of dissolved organic pools (as highlighted by Hansell et al. (2009)) led to investigation into the dissolved organic carbon (DOC) compartment in the ocean carbon cycle. As a non-sinking tracer, DOC fate is strongly linked to physical processes and its export occurs via vertical mixing and/or downwelling when it reaches intermediate waters, and via oceanic overturning circulation when it reaches the deepest layers (Hansell et al., 2002). If the early works of Copin-Montégut and Avril (1993) in the Mediterranean Sea and Carlson et al. (1994) in the Sargasso Sea were the first attempts to evaluate the export of DOC below the euphotic zone, the estimation of detrital particulate organic carbon (POC) export calculation had begun years before with the deployment of sediment traps and isotopics following (Buesseler, 1991).

The seasonal variability of DOC in the euphotic zone has been widely recorded in the sub-tropical and temperate areas of the ocean (Carlson et al., 1994; Avril, 2002; Hansell and Carlson, 2001; Santinelli et al., 2013). The results of these studies indicate a lag between DOC sources and sinks, causing summer accumulation in the upper layers due to both biotic and abiotic processes, which either alter DOC bioavailability or reduce bacterial activity. Indeed, the inefficiency of the microbial loop in organic carbon mineralization - the so-called malfunctioning microbial loop (Thingstad et al., 1997) - induces an accumulation of bioavailable DOC. This inefficiency is directly related to low phosphate availability in the upper waters of the Mediterranean Sea (Moutin et al., 2002; Van Wambeke et al., 2002; Thingstad et al., 2005; Santinelli et al., 2013).

The pathway of organic carbon not only allows to estimate the total amount of fixed carbon, but it is also crucial to determining biological pump efficiency. Modeling was chosen to adress this question, taking into account the high heterogeneity of situations encountered in the Mediterranean Sea. In line with these considerations, the biogeochemical model was designed to be potentially efficient relevant in every region (see Sect. 2). Major work has been done to estimate organic carbon export using box models (e.g. Toggweiler et al., 2003), ocean carbon-cycle models (e.g. Bopp et al., 2001;

Sarmiento et al., 1998; Maier-Reimer et al., 1996; Sarmiento and Gruber, 2006) and ecosystem models coupled with hydrodynamic models (e.g. Le Quéré et al., 2010). The objective of this paper is to fit within this framework, but at a regional the scale of the Mediterranean Basin and at high spatial and temporal resolution, with detailed description of biological processes. Several coupled models have also been developed to study the whole Mediterranean Sea, starting with the early simulation by Crispi et al. (1998); Crise et al. (1998) . The number of models for this purpose is increasing (Lazzari et al., 2013; Mattia et al., 2013; Macías et al., 2014), but to our knowledge, no modeling work has yet focused on organic carbon fluxes for the entire Mediterranean Sea. Moreover, the biogeochemical model Eco3M-MED is the only one able to analyze biogeochemical fluxes and stocks in the light of intracellular contents quotas of planktonic organisms. In this paper, we aim to further investigate organic carbon export in the Mediterranean Sea in order to quantify the associated fluxes, to study their temporal and spatial variabilities, and to provide the first estimations at this scale of the respective contributions of DOC and POC (i.e. the detrital particulate organic carbon) to carbon export. To achieve this objective, we undertook 3D biogeochemical modeling of the Mediterranean Sea using the biogeochemical model Eco3M-MED (Alekseenko et al., 2014), forced by physical simulations made with NEMO-MED12 (Beuvier et al., 2012b). The paper is organized as follows: In Sect. 2 a succinct overview of both models is given, given that they are fully detailed in the aforementioned papers. Simulation set-up and datasets used for model comparison are also presented. Sect. 3 first focuses on the assessment of the biogeochemical model outputs (nutrients, chlorophyll and primary production) through comparison with available data, then discusses results related to organic carbon inventory and export at the scale of the Mediterranean Basin, and for the discussion needs, results on intracellular quotas in phytoplankton and bacteria as well as on exudation fluxes are also presented. In Sect. 4 results on export are examined discussed in the context of previous POC and DOC export evaluations in the Mediterranean Sea and in the light of processes and intracellular quotas in phytoplankton and bacteria. Finally, a supplementary material is associated with this paper for the assessment of the biogeochemical model outputs (nutrients, chlorophyll, primary production and DOC) through comparison with available data and analysis of the main discrepancies.

2 Material and methods

2.1 The hydrodynamical model

The physical run simulation used in this work was is described by in Beuvier et al. (2012b). The model used is It has been simulated by the regional circulation model NEMOMED12 Beuvier et al. (2012a) which is part of a suite of Mediterranean regional versions of OPA and NEMO (Madec and The-NEMO-Team, 2008) as OPAMED16 (Béranger et al., 2005), OPAMED8 (Somot et al., 2006) and NEMO-MED8 (Beuvier et al., 2010).

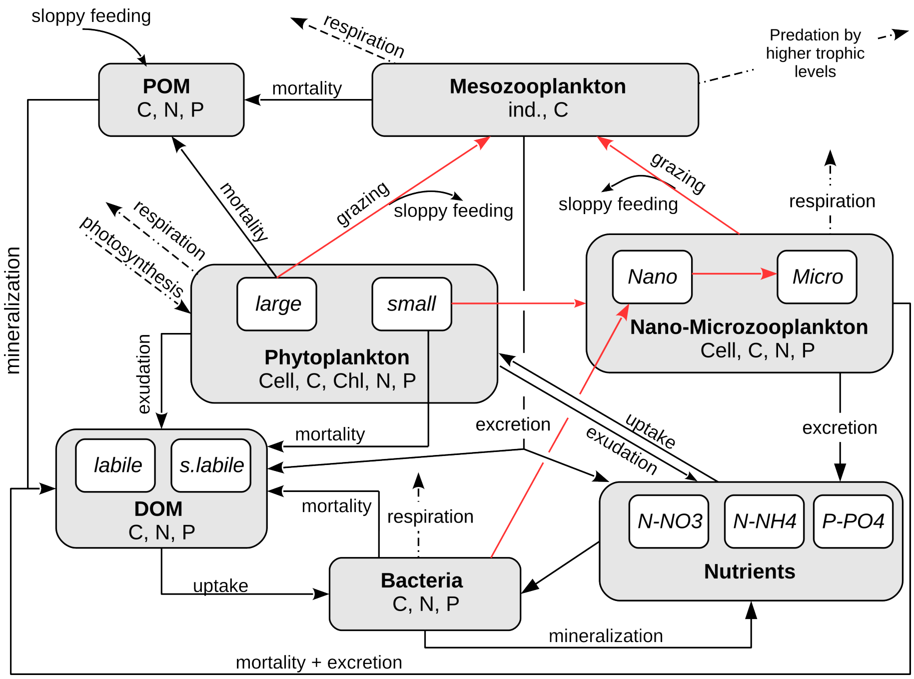

Figure 1. Conceptual diagram of the biogeochemical model Eco3M-MED. Grey boxes represent major compartments and white boxes sub-compartments. State variables for each sub-compartment are listed at the bottom of compartment boxes. Red arrows indicate grazing processes from the prey to the predator.

Model resolution is 1/12 ° (≈ 8 km) which means that most of mesoscale features are explicitely resolved, and the domain includes the whole Mediterranean Sea as well as the Atlantic Ocean West of 11°W (Fig. 2). More details of the model and its parametrization are given in Beuvier et al. (2012a). The domain configuration and model have already been used to study Western Deep Water Formation (Beuvier et al., 2012a), sensitivity test to atmospheric forcings resolution (Lebeaupin Brossier et al., 2011), transport across the Strait of Gibraltar (Soto-Navarro et al., 2014) and anthropogenic carbon stocks evaluation (Palmiéri et al., 2015).

The simulation is initiated in October 1958 with temperature and salinity data representative of the 1955–1965 period using the MEDATLAS dataset (MEDAR/MEDATLAS-Group 2002, Rixen et al., 2005). Atmosphere forcings are applied daily and come from the ARPERA dataset (Herrmann and Somot, 2008), a 55-year simulation at 50 km and daily resolutions. SST-relaxation and water-flux correction terms, as well as fresh water input from rivers and the Black Sea and Atlantic exchanges are the same as described in Beuvier et al. (2010, 2012a).

2.2 The biogeochemical model

The biogeochemical model Eco3M-MED is embedded in the Eco3M modular numerical tool (Baklouti et al., 2006b), and its structure is similar to the model presented in Alekseenko et al. (2014). Fig.

1 summarizes the interactions between the state variables through the biogeochemical processes. We chose to represent three different element cycles C, N and P allowing to reproduce the different limitations and co-limitations observed in the Mediterranean Sea. Silicium, potentially limiting in some regions (Leblanc et al., 2003) is not represented in the model, as P and N limitations are the most common ones in the Mediterranean Sea. Six different planktonic functional types (P.F.T., see Le Quéré et al. (2005) for a proper definition) are represented : 2 primary producers (phytoplankton), 1 decomposer (heterotrophic bacteria) and 3 consumers (nano-, micro- and meso-zooplanktons). The structure of the trophic web thereby includes the main P.F.T.s of the Mediterranean Sea (Siokou-Frangou et al., 2010).

Every P.F.T. is represented in terms of several biomasses (C, N, P, and Chlorophyll for producers) and an abundances (cells per unit volume), except for meso-zooplankton which is only represented through its C biomass and its abundance (individuals per unit volume). If we denote X and Y two molecules among C, N, P and Chl, this allows to dynamically calculate for each P.F.T. not only intracellular ratios Q_{XY} which are the ratio between X and Y biomasses (as this is done in previous variable stoichiometry models such as ERSEM (Baretta et al., 1995) and BFM (Vichi et al., 2007)), but intracellular quotas Q_X which are the X content per cell (expressed in mol X cell^{-1}). These intracellular quotas provide a very important additional information since intracellular ratios are only indicative of the relative quantities of a given biomass compared to another one. But for a given intracellular ratio, cells can be either depleted or repleted. By contrast, intracellular quotas give an additional information relative to cell status, that is if cells are rich or depleted in a given element. It also gives an indication of prey quality for predators. Intracellular quotas have already been used in a previous modeling study (Thingstad et al., 2005) but cell quotas of carbon were assumed fixed in the protozoa, while fixed C:N-ratios were assumed for bacteria and phytoplankton. Moreoever, this model was used without being coupled with a physical model (i.e. for the simulation of microcosm and lagrangian experiments). The producers are split into two different P.F.T.s according to their theorical size, i.e. large phytoplankton (> 10 μm) mainly encompassing diatoms, and small phytoplankton (< 10 μm) which includes picophytoplankton and the remaining nanophytoplankton. The two P.F.T.s have different parameters, (e.g. maximal growth rate, maximal uptake rate and affinity), distinct predators and they fuel different detritic pools (Fig. 1). Decomposers are represented by heterotrophic bacteria and are responsible for the organic matter mineralization, including hydrolysis of particles. Zooplankton is divided into three different size groups, heterotrophic nanoflagellate (HNF) which feeds on bacteria and small phytoplankton, ciliate which feeds on small phytoplankton and HNF, and mesozooplankton (copepods) which feeds on ciliate, HNF and large phytoplankton. Copepods are the only metazoans of the model, and mechanisms such as individual growth, egg productions or reproduction are implicitely represented (Alekseenko et al., 2014).

Eleven processes are modeled : photosynthesis, cholorophyll production, respiration, mortality, growth, uptake, grazing, excretion, exudation, nitrification and particule hydrolysis. The processes used in the model are extensively described in the aforementioned reference. However, for the needs of the present paper, we remind that POC is fueled by the natural mortality of largest organisms (mesozooplankton, diatoms and ciliates) and by the egestion of fecal pellets and sloppy feeding by mesozooplankton, and consumed by POC hydrolysis to DOC. The DOC pool has many inputs (phytoplankton exudation, zooplankton excretion, mortality of small organisms, POC hydrolysis) and a single output (uptake by bacteria). The formulations of most of the biogeochemical processes, for which details are extensively given in Baklouti et al. (2006a, 2011); Mauriac et al. (2011), and Alekseenko et al. (2014), follow cell level mechanistic considerations. follow cell level mechanistic considerations, and intracellular concentrations, quotas and ratios are explicitely calculated Intracellular ratios (Q_{XY}) and intracellular quotas (Q_X) are used to regulate growth via Droop's quota function (Droop, 1968) and net uptake and grazing rates via Geider's limitation formulation (Geider et al., 1998). For example, the specific growth rate (i.e. the division rate) μ of all unicellulars in the model is given by the following equation:

$$\mu = \mu^{\max} \min_{X \in \{\mathrm{C, N, P}\}} \left(1 - \frac{Q_X^{min}}{Q_X}\right) \tag{1}$$

where $\mu^{\max}$ is the maximum division rate and $Q^{\min_X}$ the minimum intracellular X quota.

Grazing, primary production and uptake rates are controlled firstly by the organism environment (either preys or nutrient concentration, or light availibility). Secondly, the internal cell status drives a feedback regulation of the net incorporated biomass. The uptaken extra is either released in its initial form or exuded in the form of DOM. The same assumptions are applied to estimate excretion (ammonium, phosphate), and fecal pellets production. Furthermore, 10 % of material grazed by mesozooplankton directly fuels the particulate organic matter stock, to represent sloppy feeding. Respiration rates are estimated via energy costs for every plankton activity (Alekseenko et al., 2014). Nitrification is represented through first order kinetics while particulate hydrolysis function depends on bacteria intracellular quotas (POC hydrolysis increases with bacterial C-limitation). Grazing by higher trophic levels is implicitely taken into account via a quadratic mortality affecting only mesozooplankton. Grazing function is a Holling II type (Holling, 1959; Kooijman, 2000) for multiple preys. The only difference with Alekseenko et al. (2014) configuration lies in the formulation used to represent predator preferences for multiple preys. We here used the "Kill The Winner" (KTW) formulation depicted in Vallina et al. (2014) which combines active-switching (i.e. the preference of a predator for a given prey depends on prey density) and an ingestion rate always increasing with the total biomass of preys. This active-switching formulation was used to preserve foodweb diversity (e.g Prowe et al., 2012) and to prevent unrealistic predator-prey oscillations.

Since the model relies on mechanistic basis, parameters are mainly physiological (and measurable) and they were either taken from literature or derived from other parameters on the basis of greater consistency between parameters. For example, maximum intracellular quotas are inferred

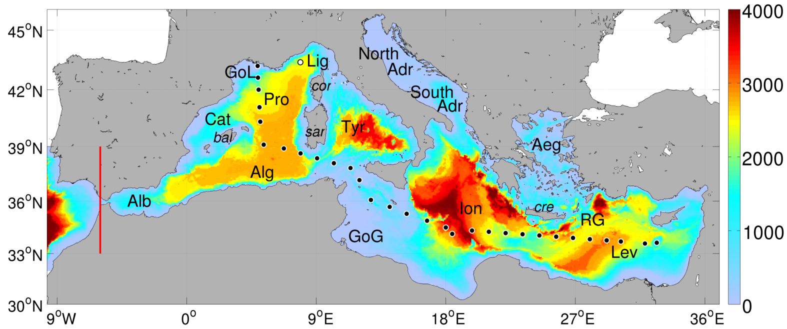

Figure 2. Bathymetry of the grid in meters, black dots represent the BOUM cruise stations (Moutin et al., 2012a) while white dot is DyFaMed position (Marty and Chiavérini, 2010). The area West of the red line constitutes the buffer-zone. Acronymes indicates different sub-basin names and islands (in italic). Terminology is taken from Millot and Taupier-Letage (2005). From West to East, **Alb** stands for Alboran Sea, **Cat** the Catalan Sea, **GoL** for the Gulf of Lions, **Pro** the Provencal sub-basin, **Alg** the Algerian basin, **Lig** for the Ligurian Sea, **Tyr** for the Tyrrhenian Sea, **GoG** for the Gulf of Gabes, **North Adr** and **South Adr** for the North and South Adriatic Sea respectively, **Ion** for the Ionian sub-basin, **Aeg** for the Aegan Sea, **Lev** the Levantine sub-basin and **RG** the Rhodes Gyre. Major islands names are also plotted, *bal* stands for the Balearic islands, *sar* for Sardinia, *Cor* for corsica, *cre* for Crete.

from minimum ones as done in Thingstad et al. (2005). Another example lies in the relationship between the maximum uptake rate of a given element which is the product of the maximum specific growth rate and the maximum intracellular quota in that element. Other examples as well as the whole set of parameters are given in Alekseenko et al. (2014).

2.3 Model coupling

The models NEMO and Eco3M-MED have been associated for the first time. The coupling between the hydrodynamic and biogeochemical models is offline, i.e. biological retroaction on physics is not taken into account. Daily-averaged water velocities were used for the advection of biogeochemical tracers, using a MUSCL scheme (horizontal and vertical diffusion fluxes are calculated according to a centered scheme). The time-step used for the numerical integration of the tracer conservation equations equals 1200 s. A sinking velocity of 2 m d^{-1} is applied only on the particulate organic pool (i.e. the detrital compartment). This compartment aims at representating particles with different sizes and sinking velocities and the value of 2 m d^{-1} is within the usual range found in litterature (Vichi et al., 2007; Fasham et al., 2006). Light attenuation in the water column is modeled via the formulation of Morel (1988).

2.4 Initial and boundary biogeochemical conditions

Initial nutrient and chlorophyll fields are derived from annual means of the Mediterranean Sea climatology (Schaap and Lowry, 2010). The remaining biogeochemical variables are derived from chlorophyll using conversion factors derived from published works (see Alekseenko et al. (2014) for details).

A "buffer-zone" has been defined between the domain western boundary and the Gibraltar Strait (from 11°W to 6°W), in which a damping procedure towards the Atlantic conditions has been applied. The restoring time is 2 days West of 7.5°W, lineary increasing to 90 days from 7.5°W to 6°W (Fig. 2). Atlantic nutrient concentrations come from the World Ocean Atlas monthly climatology (Garcia et al., 2006), so that the nutrients damping in the "buffer-zone" takes into account the nutrients monthly variability. Given the imprecisions in phosphate measurements, we decided to compute phosphate profiles from that of nitrate by imposing a redfield ratio of 16 to be more coherent with observed NO_3:PO_4 ratios in this region (Gómez, 2003). Chlorophyll concentrations were not provided in this database. We therefore used in situ data from the SeaDataNet database to create a mean vertical chlorophyll profile for the Atlantic, and then used a climatology of surface chlorophyll from the GlobColour product in this region to represent an annual cycle of the chlorophyll vertical profile. The remaining Atlantic biogeochemical variables were derived from chlorophyll using the same procedure as for initial conditions.

Nutrient (NO_3 and PO_4) inputs from riverine influx and coastal runoffs are derived from Ludwig et al. (2009), following the same procedure as for the riverine freshwater inputs in the circulation model (Beuvier et al., 2010, 2012b). The nutrient influx of the 29 rivers included in the RivDis database (Vörösmarty et al., 1996) are taken into account in the simulation, while the nutrients of the remaining rivers from Ludwig et al. (2009) database are averaged for every sub-basin and distributed along their respective sub-basin's coast as coastal runoffs. Dissolved organic carbon inputs in the Mediterranean Sea are distributed in every sub-basin according to the riverine DOC estimates of Ludwig (1996) (a total of $\sim$ 1.8 Tg C y^{-1} in the whole Mediterranean Sea). Sub-basin DOC inputs were then distributed among fluvial estuarines and coastal runoffs to match circulation model freshwater geographical distribution (Palmiéri, 2014; Palmiéri et al., in prep).

Mass exchanges with the Black Sea at the Dardanelles Strait are treated as river inputs, with nutrients and DOC input concentrations provided by the SESAME project (Tugrul and Besiktepe, 2007; Meador et al., 2010). But, since NO_3 budget indicates a negative net flux of NO_3 the Dardanelles Strait (i.e. exiting from the Mediterranean), NO_3 flux at Dardanelles is set to zero and the outcome is transferred on the Aegean sub-basin's runoffs. These runoffs are artificially reduced in order to keep the riverine budget of NO_3 in the Aegean sub-basin realistic.

2.5 Simulation set-up

Using the biogeochemical initial conditions defined in Sect. 2.4, we have conducted a 5 years simulation using physical forcings from the years 1973-1977. This first simulation was considered as a 'spin-up', in order to reduce the impact of state variables adjustment in the simulations. It has deliberately been done enough before the Eastern Mediterranean Transient period (starting around 1991) which is not stable enough to be chosen as a spin-up period. Moreover, due to high computational costs, it was not possible to run this first simulation until the year 1996, and we used the final biogeochemical state of this spin-up as initial conditions for a second simulation running from 1996 to 2012. In this second simulation, only the years following 1998 are considered, since the first 3 years were treated as an additional spin-up beyond which the stability of the run was ensured (i.e. no drift could be observed).

2.6 Data description

The present work intends to study and to quantify organic carbon export fluxes with a 3D physical-biogeochemical model. For this purpose, our first objective was to assess the reliability of our model by examining the agreement between different model outputs and corresponding available data : chlorophyll, nutrients, DOC concentrations and primary production rates.

Three type of comparisons were undertaken : (i) at basin scale, using surface chlorophyll fields provided by satellite for comparisons at different seasons (ii) at basin scale, using BOUM cruise transect as a "snapshot" to compare nutrients and DOC vertical profiles during the stratified period (iii) at a local scale using the time series data collected at DyFaMed station

2.6.1 Chlorophyll data derived from satellite

Among the specificities of the Mediterranean Sea, its strong oligotrophy and the major influence of colored dissolved organic matter, make the use of classical satellite chlorophyll products difficult (e.g. Claustre et al., 2002). Several algorithms have already been developped (Bosc et al., 2004; D'Ortenzio et al., 2002; Volpe et al., 2007), using different satellite reflectances and datasets. Here, we used a daily surface chlorophyll product delivered by the Myocean project (http://www.myocean.eu). In this product, chorophyll concentrations have been derived using the MEDOC4 algorithm developped by Volpe et al. (2007). and applied to multi-sensor marines reflectance produced in the frame of the Climate Change Initiative of the European Spatial Agency (CCI-ESA http://www.esa-oceancolour-cci.org/). This algorithm has been built using a large dataset of in situ chlorophyll concentrations collected and reflectance measurements from 3 satellites (Seawifs, MERIS and MODIS), constituting an homogeneous serie from September 1997 to March 2012. Daily chlorophyll maps are then aggregated into eight-days maps (i.e. 46 per year) to reduce data gaps. Besides, a spatial smoothing operator is applied on 5 pixel squares (≈ 40 km) with distance-derived weights to reduce spatial noise.

2.6.2 The BOUM cruise data

The BOUM cruise took place during summer 2008 (from June 16 to July 20) and crossed both the Western and Eastern basins of the Mediterranean Sea (Moutin et al., 2012a). The data acquired during this cruise give a unique picture of the biogeochemical status of the Mediterranean Sea since many biogeochemical variables have been observed. Measurements of nutrients and DOC concentrations were used to perform a basin-scale observation comparison during the summer stratified period with the corresponding model outputs obtained at the same dates as the cruise, and averaged over this period.

2.6.3 The DyFaMed station data

The DyFaMed station is located in the Ligurian Sea at 7.9°E and 43.4°N , 50 km off Cap-Ferrat (Fig. 2) and is isolated from coastal inputs by the Mediterranean Northern Current. A strong winter mixing is observed in this area, although less intense than the deep convection occuring in the Provencal sub-basin (Marshall and Schott, 1999). Nutrients (Pasqueron de Fommervault et al., 2015), chlorophyll (Marty et al., 2008), dissolved organic carbon (Avril, 2002) and primary production rates (Marty et al., 2008) time series were used for comparison. The comparison of the model outputs with DyFaMed time series can be done through different methods. The simplest one consists in using a single grid point which is the nearest from the DyFaMed station location. This implies that the model perfectly reproduces spatial patterns in this region, which is obviously never the case. On the other hand, the use of model outputs averaged on several grid points around DyFaMed station amounts to dampening signal variability. We finally chose to use the nearest gridpoint to DyFaMed station, while assessing spatial variability in the 8 neighbouring grid points (Table 2).

3 Results

3.1 Organic carbon inventory and export

3.1.1 Dissolved organic carbon inventory

In what follows, mDOC refers to the modeled dissolved organic carbon integrated over the first 100 m of the water column. Seasonal variations of mDOC are given in Fig. 3. Low mDOC values (< 1 mol m^{-2}) are observed throughout the year in the region extending from the Gibraltar Strait to the Alboran Sea (and up to the Balearic Islands), the North Levantine basin, and in some well marked patches between Corsica and Sicilia Islands, and East of the strait of Bonifacio structures in the Thyrrenian Sea. On the opposite, very high mDOC values (up to 5 mol m^{-2}) can be found

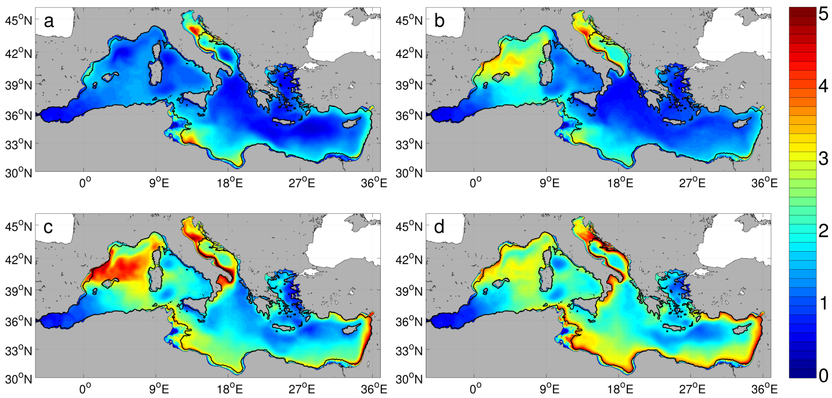

Figure 3. Modeled dissolved organic carbon inventory (mol m^{-2}) integrated over the first 100 m. Maps are averaged over the 2000-2012 period in (a) winter (Dec.-Feb.), (b) spring (Mar.-May), (c) summer (Jun.-Aug.), (d) autumn (Sept.-Nov.). Black lines are the 100 m isolines.

all along the year in the North Adriatic Sea and along the Lybian Coast. Apart from these regions, mDOC is low everywhere (below 2 mol m^{-2}) in winter (Fig. 3 a), and this is also true in spring except in the region of the spring bloom in the Provencal sub-basin The highest mDOC seasonal variations are observed in coastal areas (especially along the and in the South Ionian Sea. Elsewhere, mDOC variations are high in the whole Ionian Sea, the Tyrrhenian Sea, the North Adriatic Sea, the Provencal sub-basin and the Algerian sub-basin. In the Western basin, highest DOC concentrations are generally observed in summer, with values reaching 4 mol m^{-2} in the bloom region of the Liguro-Provencal sub-basin. In the Eastern basin, they are reached in autumn and mostly concern the Adriatic Sea, and the regions along the southern and eastern coasts.

During spring (Fig. 3 b), relatively high mDOC values are observed in the Liguro-Provencal sub-basin (> 3 mol m^{-2}) and in the Adriatic Sea (> 4 mol m^{-2}). During summer (Fig. 3 c), mDOC in the Western basin is mainly above 3 mol m^{-2} with values reaching 4 mol m^{-2} in its central part. Values are lower (about 2 mol m^{-2}) in the Tyrrhenian Sea. In the Eastern basin, mDOC values reach 2 mol m^{-2} in the Ionian basin, and increase southward to reach 3 mol m^{-2} along the Libyan Coast. Along the Eastern coast of the Levantine basin, high values (> 5 mol m $^{-2}$) are obtained. During autumn (Fig. 3 d), mDOC values are high in almost every coastal areas. In the whole basin, mDOC is higher than 2.5 mol m^{-2}, except in the central Levantine basin where it is below 2 mol m^{-2}.

Regular measurements of total DOC (i.e. including refractory and semi-refractory pools) performed at DyFaMed site (Avril, 2002) were used for comparison. Since the model only provides the labile and semi-labile DOC pools, the in situ DOC concentration measured in deep water (> 1000 m), which can be considered as refractory DOC, has been added to the model DOC output. Moreover, since our run does not cover the period of in situ data, we decided to work on a climatology of DOC vertical profiles: bi-monthly mean, maximal and minimal DOC values were calculated and compared (Fig. 24).

The climatology of DOC at DyFaMed proposed by Avril (2002) is divided into three periods. During spring, DOC stocks increase just after the bloom and DOC is related to the POC hydrolysis at depth. During summer, stratification isolates the surface layer where DOC accumulates due to the activity of small phytoplankton and to reduced bacterial activity. Then, during winter the water column is mixed.

At the DyFaMed grid point, model outputs also show a DOC increase during spring (April-May), but close to the surface. Then, in summer, the DOC production rate is lower than in spring but still significant and limited to the upper layers. Surface DOC stocks decrease (as of September) with mixing. DOC seasonal variations of both the model and observations are maximal at surface, however modeled DOC variations rapidly decrease with depth and they are lower than observations at 150 m depth. As a consequence, the modeled DOC vertical gradient is higher than the observed one, particularly in summer. DOC stocks variations are higher in the model : integrated DOC within the first 100 m ranges between 5.5 and 9.4 mol m^{-2} for the model, and between 7.2 and 8.7 mol m^{-2} for in situ data.

3.1.2 Particulate organic carbon inventory

In what follows, mPOC refers to the modeled particulate organic carbon integrated over the first 100 m of the water column. Seasonal variations of mPOC are given in Fig. 4. Unlike mDOC, mPOC highest values are observed in winter and spring. This is mostly true for the Western basin since, Some major differences in the mPOC seasonal signal exist between basins. in the Eastern basin, mPOC remains low ($<$ 0.05 mol m^{-2}) all over the year, except for the Adriatic Sea and a local maximum in the Rhodes Gyre distinguishable in spring (May-June) . mPOC seasonal variations are limited to the Western basin (especially in the Alboran Sea and the (Liguro-Provencal sub-basin)), and the Adriatic Sea. During winter (Fig. 4 a), the highest values of mPOC ($>$ 0.5 mol m^{-2}) are found in the region of the Alboran Sea and the surrounding Balearic Islands and also in the Liguro-Provencal sub-basin though with much lower concentrations. A patch of values around 0.3 mol m^{-2} is observed in the Provencal sub-basin. In the Adriatic Sea, mPOC is in the range [0.1;0.2] mol m^{-2}. Elsewhere, mPOC is very low ($<$ 0.2 mol m^{-2}). During spring (Fig. 4 b), the maximum mPOC is observed in the region of the bloom in the Provencal sub-basin ($\approx$ 0.4 mol m^{-2}) and the North Adriatic Sea. In the Western basin, mPOC is higher than 0.2 mol m^{-2} and reach 0.4 mol m^{-2} in the Alboran Sea, except in the Tyrrhenian Sea where it remains below 0.05 mol m^{-2}. In the Eastern basin, values of mPOC are generally below 0.05 mol m^{-2}, although in the Rhodes Gyre, values up to 0.15 mol m^{-2} are calculated. Values from 0.2 to 0.5 mol m^{-2} are obtained in the whole Adriatic Sea. During summer and autumn (Fig. 4 c and d), overall values are low ($<$ 0.05 mol m^{-2}), except in the Alboran Sea (where values reach 0.3 mol m^{-2}) and in the North Adriatic Sea. During autumn

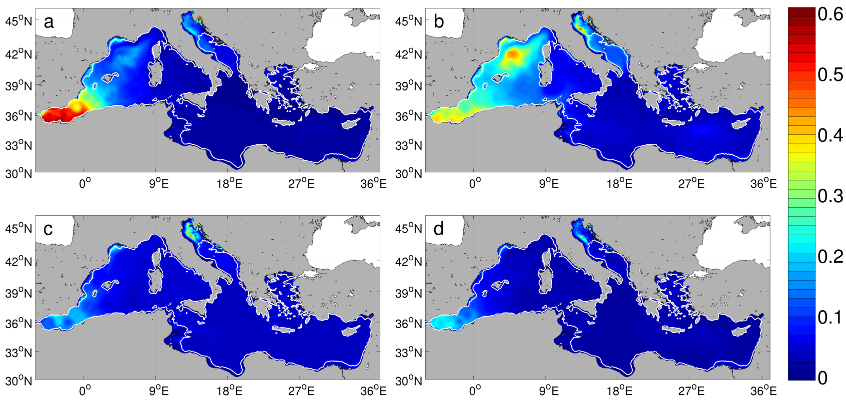

Figure 4. Modeled particulate organic carbon inventory (mol m^{-2}) integrated over the first 100 m. Maps are averaged over the 2000-2012 period in (a) winter (Dec.-Feb.), (b) spring (Mar.-May), (c) summer (Jun.-Aug.), (d) autumn (Sept.-Nov.). White lines are the 0 m and 100 m isolines.

(Fig. 4 d) , the patterns are close to the ones in summer except that values are slighlty higher (about 0.3 mol m^{-2}) in the Alboran Sea.

In the latter, mPOC declines almost towards zero in summer, and starts increasing in late winter (March). The dynamics in the Adriatic Sea is quite similar, except in the North where a maximum mPOC is calculated in summer. In the Western Alboran Sea (West 0°), mean mPOC remains above zero all over the year : it starts increasing in early winter (January) and remains relatively high until the summer decrease.

3.1.3 Dissolved and particulate organic carbon export

Organic carbon fluxes are computed 100 m and 200 m by adding the contribution of advection (vertical velocity and settling velocity for POC) and diffusion (implicitely representing turbulence and convection mixing) processes across the grid. Negative fluxes account for downward fluxes. For clarity, modeled fluxes will be referred to as F_{DOC} , F_{POC} and F_{OC} as the sum of the latter two. F_{DOC} and F_{POC} have been computed at 100 m and 200 m so as to include most of the productive layer and to allow the comparison in space and time between regions. These depths are also used in several other modeling studies (Lévy et al., 1998; Bopp et al., 2001).

The yearly amount of mOC export at 100 m is equal to 48.4 MtC y^{-1}. The Eastern basin is the main contributor to this export with a total export of 28.7 against 19.7 MtC y^{-1} for the western basin. mDOC export is equal to 38.8 MtC y^{-1}, and comparatively, river inputs of mDOC is equal to 1.8 MtC y^{-1}, thereby representing only less than 5% of the exported mDOC. mDOC contribution to the total organic carbon flux is dominant. In the Western basin, the global amounts of exported mPOC and mDOC below 100 m are respectively 7.0 MtC y^{-1} and 12.7 MtC y^{-1}, meaning that 64

% of this export is due to DOC. In the Eastern basin, DOC is responsible of 90 % of the organic carbon export below 100 m, with an annual flux of 26.1 (against 2.6 for POC) MtC y^{-1}. DOC export occurs in both Western and Eastern basins in relative similar proportion compared to POC export.

3.1.4 Spatial variability of export fluxes

Mean F_{OC} over the whole basin equals -22.8 gC m^{-2} y^{-1}, (median of -17.8 gC m^{-2} y^{-1}). 95 % of the flux values are within the range - 80 to 12 gC m^{-2} y^{-1} with extreme values indicating a but a large spatial variability can be observed in Fig. 5. According to the model, Hence, the main regions of organic carbon mOC export are the Liguro-Provencal sub-basin, the Alboran Sea, the southern continental slopes and the Adriatic Sea.

In the Western basin, 95 % of downward F_{DOC} values range from 1 to 69 gC m^{-2} y^{-1} with a stronger variability within coastal and shallow areas. high positive values (i.e. upward) of F_{DOC} are simulated along the French and Spanish coasts, the entrance of the Sicilian Strait and North-East of Corsica. Excluding these areas, the highest downward fluxes of DOC highlighted by the black contours in Fig. 5 top are calculated in the Provencal sub-basin (especially in the region of deep convection), the North of the Balearic Islands and along the Algerian slope, where downward F_{DOC} can be higher than 60 gC m^{-2} y^{-1}. In the Algerian basin, the Balearic Sea and the Tyrrhenian Sea, F_{DOC} values are quite homogeneous and range from -5 to -15 gC m^{-2} y^{-1}.

In the Eastern basin, 95 % of the downward F_{DOC} values range from 4 to 74 gC m^{-2} y^{-1}. the complexity of topography and hydrodynamical regimes in the Aegan Sea may explain the high heterogeneity of the fluxes calculated in this region that are difficult to interpret. Highest downward F_{DOC} values are located along the continental slopes from the Lybian to the Turkish coasts and in the Adriatic Sea where the median value is around -25 gC m^{-2} y^{-1}. F_{DOC} is more homogeneous in the open sea, with a median of -17 gC m^{-2} y^{-1}.

A strong difference exists between the Western and Eastern basins regarding F_{POC} at 100 m. Mean value of downward F_{POC} over the Western basin is -9.8 gC.m^{-2}.y^{-1} (median of -7.8 gC m^{-2} y^{-1}) and -2.4 gC m^{-2} y^{-1} (median of -1.9 gC m^{-2} y^{-1}) in the Eastern basin (Fig. 5 bottom).

In the Western basin, F_{POC} is the highest (see black contour in Fig. 5 bottom), in the Alboran Sea, particularly in the South East of the easily identifiable anticyclonic eddies. Following the pathway of the Atlantic waters, downward F_{POC} values decrease to reach absolute values lower than 5 gC m^{-2} y^{-1} in the Tyrrhenian Sea. In the Provencal basin high POC fluxes linked to the deep convection, with values ranging from -15 to -30 gC m^{-2} y^{-1} are modeled. All over the Eastern basin, F_{POC} is low (around -1.9 gC m^{-2} y^{-1}), except in the Adriatic Sea. where the mean F_{POC} equals -4.7 gC m^{-2} y^{-1}.

Finally, as suggested by Fig. 5, the spatial correlation between POC and DOC fluxes is weak almost everywhere. Regions of high POC or (DOC) export (see contours in Fig. 5) generally do not

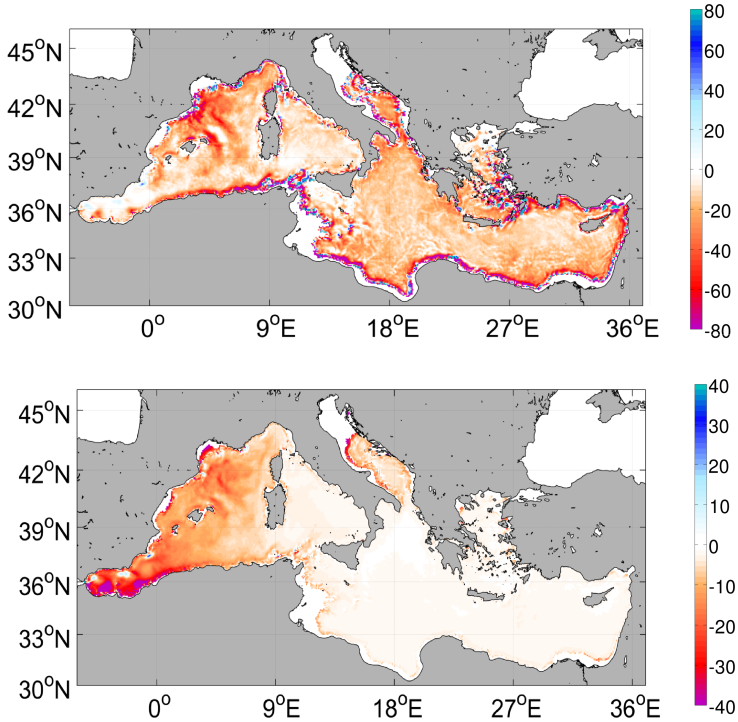

Figure 5. Maps of modeled annual DOC fluxes (top) and POC fluxes (bottom) below the 100 m layer in gC m^{-2} y^{-1}. Note the colorscale differences. Negative (red) means a downward flux. Black lines are the contour of the 8th decile of downward fluxes for DOC (-28.3 gC m^{-2} y^{-1}) and for POC (-7.8 gC m^{-2} y^{-1}).

match. The only areas associated with both high POC and DOC exports are the Algerian coast, the Adriatic coast, the regions of deep convection and a band east of the Balearic Islands.

3.1.5 Seasonal variability

The seasonal variability and the spatial distribution of F_{DOC} and F_{POC} differ significantly (Fig. 6 and 7). Significative DOC fluxes generally occur in winter (Fig. 6). Maximum values of F_{DOC} are reached in early winter in the Provencal sub-basin and along the continental slopes from autumn to early spring. In several areas (Tyrrhenian and Adriatic Seas, Levantine and Ionian basins), high downward F_{DOC} values are observed in winter while they are almost null during the rest of the year.

DOC export takes place when DOC rich surface waters plunge or are mixed with poorer deeper waters. Bacteria are the first consumers of DOC, their internal status shapes DOC patterns at basin scale and DOC accumulation is due to an availability beyond bacterial carbon needs. When the relative C quota of bacteria is the lowest (i.e. lower than N and P quotas), bacteria growth and

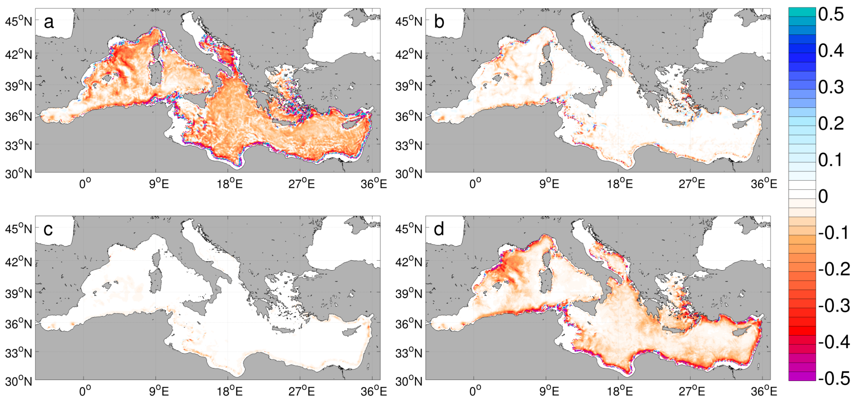

Figure 6. Maps of modeled DOC fluxes across the 100 m layer (F_{DOC}) in gC m^{-2} d^{-1} in (a) winter (Dec.-Feb.), (b) spring (Mar.-May), (c) summer (Jun.-Aug.), (d) autumn (Sept.-Nov.). Negative (red) means a downward flux.

sustainibility are limited by the amount of DOC in their local environment, meaning that bacterial needs in DOC are higher than the available DOC in water. Therefore intracellular quotas of bacteria can therefore help in the identification of regions of potential DOC accumulation.

Fig. **??** aims to resume the connection between bacteria and DOC at 100 m depth. In most regions bacteria are depleted in carbon and any input of DOC would lead to an increase in bacterial activity and a consumption of this pool. On the opposite in some regions bacteria are rarely limited by carbon, particularly along continenal slopes in the Eastern basin and in the south Ionian Sea (south of 34°N). In these areas, DOC may not be consumed even at 100 m depth and export may then occurs during the whole year.

High absolute values of F_{POC} at 100 m are calculated from winter to spring in the Alboran Sea and the Provencal sub-basin (Fig. 7). In the regions associated with the highest downward F_{POC} values (West of 7°E, see Fig. 5 bottom), the maximum occurs in late winter (February-March) in the Alboran Sea, and in spring (March-April) in the Algerian Sea and the Provencal sub-basin. Elsewhere, the maxima are in spring in the Tyrrhenian Sea, the Levantine basins (except for the Rhodes Gyre where the maximum is earlier in winter) and in the Adriatic Sea. POC export in the Eastern basin (excluding the Adriatic Sea) is very weak (even in the Rhodes Gyre). given the fact that POC concentrations stay very low (see paragraph 3.1.5). Our results may however underestimate the actual POC flux in the Eastern bassin as seen when comparing with observation made with sediment traps (see Discussion).

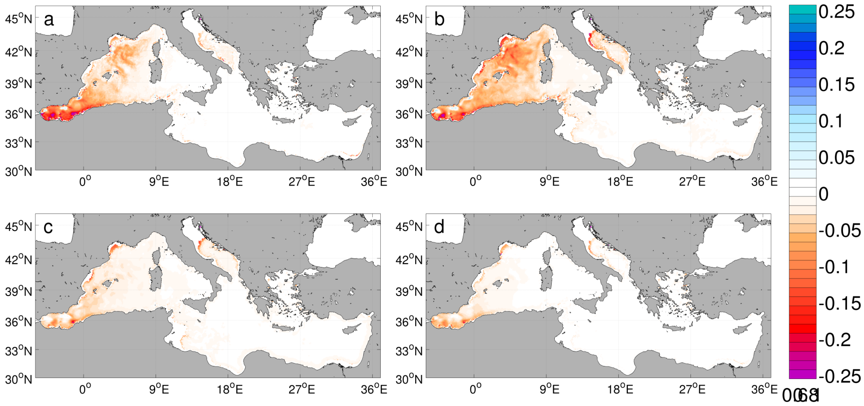

Figure 7. Maps of modeled POC fluxes across the 100 m layer F_{POC} in gC m^{-2} d^{-1} in (a) winter (Dec.-Feb.), (b) spring (Mar.-May), (c) summer (Jun.-Aug.), (d) autumn (Sept.-Nov.). Negative (red) means a downward flux.

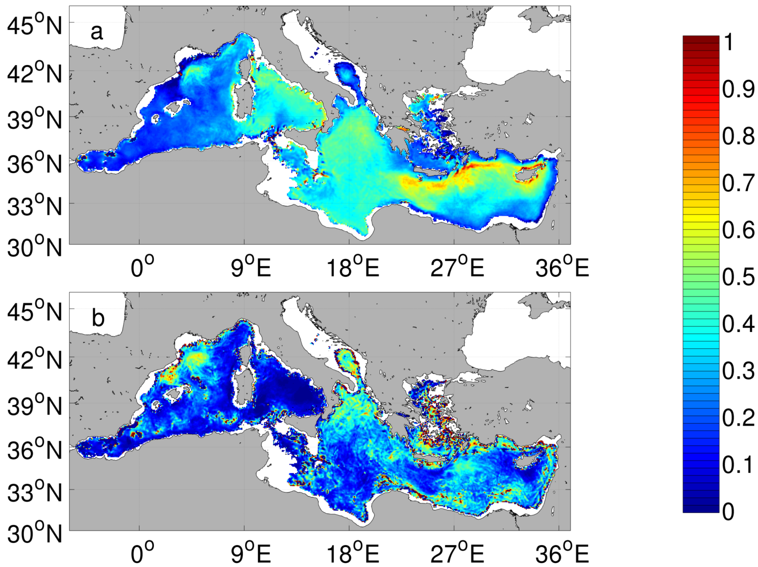

Figure 8. Ratio between export fluxes at 200 m and at 100 m (a) for POC, (b) for DOC.

3.1.6 Export below 200 m

Below 100 m, organic carbon is progressively consumed via the bacterial activity and respiration. At 200 m, the calculated mean export fluxes of total organic carbon are reduced by almost 87 % and 64 % compared to those at 100 m, respectively in the Western and Eastern basins. However, the ratio between export at these two depths is highly variable, depending on the region and the form of organic carbon (see Fig. 8).

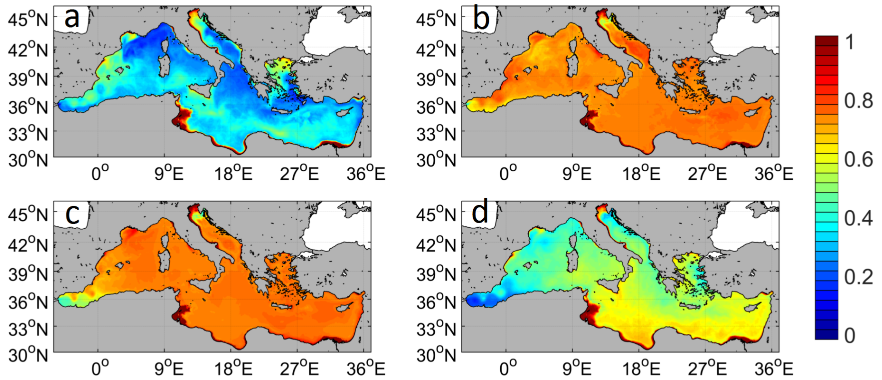

Figure 9. Seasonal variations of mean 0-50 m carbon relative quotas in small phytoplankton: (a) winter (Dec.-Feb.), (b) spring (Mar.-May), (c) summer (Jun.-Aug.), (d) autumn (Sept.-Nov.). Relative quotas are equal to 0 when the quota is mimimum (i.e. when Q_C = Q_C^{min}) and equal to 1 when the quota is maximum (i.e. when Q_C = Q_C^{max})

For POC (Fig. 8 a), the 200 m to 100 m ratio is lower than 0.25 (i.e. only 25 % of the carbon exported at 100 m goes below 200 m) in a region including the Alboran Sea, the West Algerian Sea and the Balearic Sea where POC export at 100 m is high (see Fig. 5 bottom). This ratio is slighly higher but still below 0.3 for the central Algerian Sea and the Adriatic Sea, the Provencal sub-basin is the only region of high export below 200 m with a ratio about 0.4. In the Tyrrhenian Sea, the Ionian and Levantine basins, ratio ranges between 0.4 and 0.8 but are associated with low downward POC fluxes below 100 m.

For DOC (Fig. 8 b), the ratio is more spatially variable, and in some regions the ratio is higher than 0.4 : the Provencal sub-basin, continental slopes in the Levantine basin, the North Ionian basin, the Rhodes Gyre and the Adriatic Sea. Some patches of high ratios are also visible close to the Algerian Coast. Elsewhere the ratio ranges from almost zero (Tyrrhenian Sea, the Alboran Sea) to 0.2 in the Eastern basin.

3.2 Intracellular quotas in bacteria and phytoplankton

Intracellular quotas in phytoplankton and bacteria are required for a further analysis of POC and DOC export fluxes and presented in what follows. Carbon quota (Q_C) in small phytoplankton is the highest in spring and summer in almost all the Mediterranean Sea, though slightly lower in spring in the western basin than in the eastern one, especially in the bloom region (Fig. 9). In autumn, though Q_C has decreased in nearly all the Mediterranean Sea, Q_C values along the southern and eastern coasts of the Eastern basin are significantly higher than in the rest of the open sea.

The seasonal signal of the P quota (Q_P) in small phytoplankton is nearly the opposite of Q_C one, with the highest Q_P values in autumn and mostly in winter in nearly the whole Mediterranean Basin,

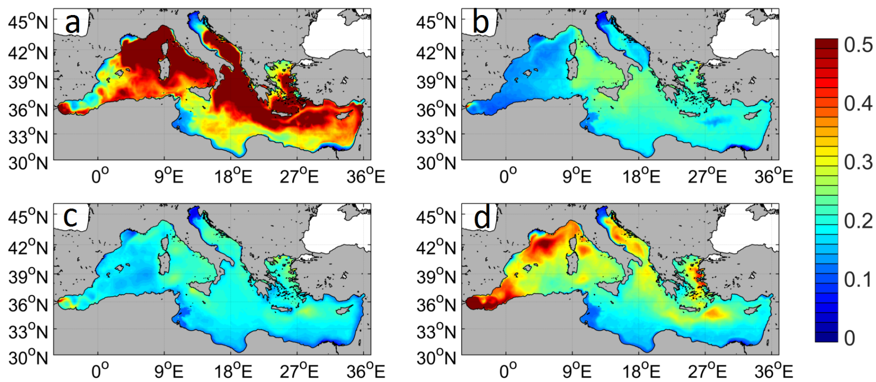

Figure 10. Seasonal variations of mean 0-50 m phosphorous relative quotas in small phytoplankton: (a) winter (Dec.-Feb.), (b) spring (Mar.-May), (c) summer (Jun.-Aug.), (d) autumn (Sept.-Nov.). Relative quotas are equal to 0 when the quota is mimimum (i.e. when $Q_P = Q_P^{min}$) and equal to 1 when the quota is maximum (i.e. when $Q_P = Q_P^{max}$)

and the lowest ones in spring and summer (Fig. 10). All year long, Q_P values are lower along the southern and eastern coasts than in the rest of the Eastern basin.

Bacteria Q_C generally increases from winter to summer in most of the Mediterranean Basin (Fig. 11). In autumn, the decrease in Q_C is observed everywhere except along the same already identified region (namely along the southern and eastern coasts of the Easten basin). All year round, Q_C values are higher in this region than in the rest of the basin and even reach the $Q_C^{\max}$ value in summer and autumn thus indicating that carbon needs for bacteria growth are fully satisfied. In the deep convection regions (Liguro-Provencal sub-basin, Adriatic, Rhodes Gyre region), and in some eddies well identified in the Alboran and Thyrennian seas, carbon quota is generally lower than in the surroundings water, especially in autumn.

Bacteria Q_P values are very low everywhere in spring and summer except in the latter regions. The minimum Q_P values (i.e. the highest bacterial P-limitation) are observed in spring in the Western basin, while they are reached in summer in the Eastern basin. As for phytoplankton, Q_P values are lower all year round along the southern and eastern coasts than in the rest of the Eastern basin.

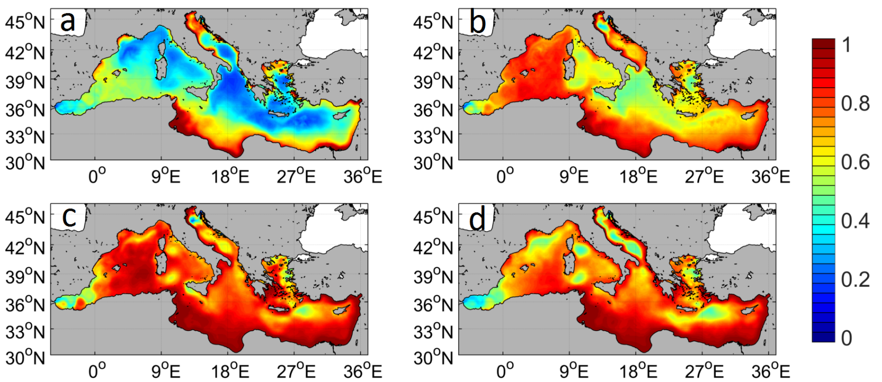

Figure 11. Seasonal variations of mean 0-50 m carbon relative quotas in bacteria: (a) winter (Dec.-Feb.), (b) spring (Mar.-May), (c) summer (Jun.-Aug.), (d) autumn (Sept.-Nov.). Relative quotas are equal to 0 when the quota is mimimum (i.e. when $Q_C = Q_C^{min}$) and equal to 1 when the quota is maximum (i.e. when $Q_C = Q_C^{max}$)

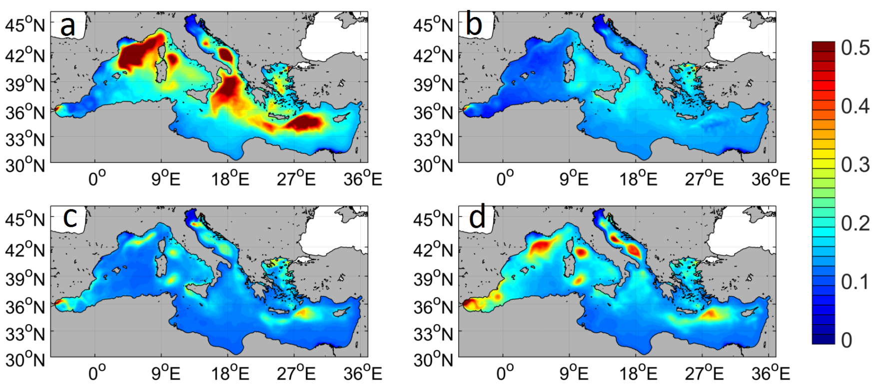

Figure 12. Seasonal variations of mean 0-50 m phosphorous relative quotas in bacteria: (a) winter (Dec.-Feb.), (b) spring (Mar.-May), (c) summer (Jun.-Aug.), (d) autumn (Sept.-Nov.). Relative quotas are equal to 0 when the quota is mimimum (i.e. when $Q_P = Q_P^{min}$) and equal to 1 when the quota is maximum (i.e. when $Q_P = Q_P^{max}$)

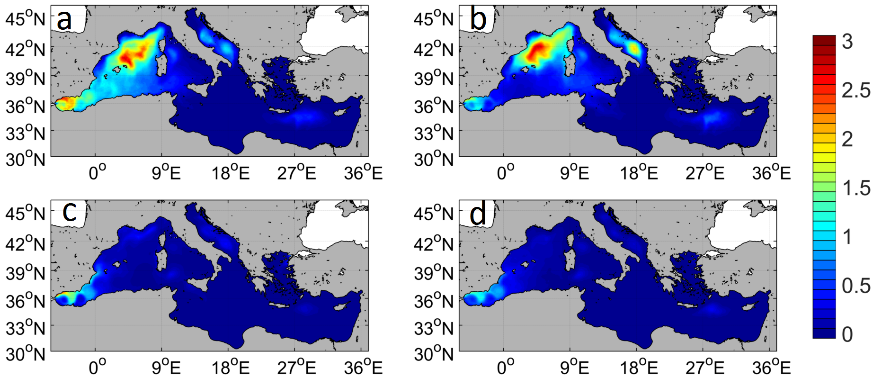

Figure 13. Seasonal variations of DOC mean 0-100 m exudation cumulated flux by large phytoplankton (in mol $C.m^{-2}$).

3.3 DOC exudation by phytoplankton

DOC exudation by large phytoplankton mainly occurs in the bloom region of the Western basin (especially in the deep convection zone), in (late) winter and spring where cumulated fluxes are up to 2.8 mol $C.m^{-2}$ (Fig. 13). Elsewhere, exudation fluxes are very low all along the year, except in the Alboran Sea, two eddies of the Adriatic Sea and in the Rhodes gyre region.

The seasonality and the spatial patterns of DOC exudation flux by small phytoplankton are rather different. The highest mDOC exudation fluxes are modeled in spring in the Western basin, especially in the Gulf of Lions and the deep convection zone where cumulated fluxes up to 3 mol $C.m^{-2}$. In the Eastern basin, the highest fluxes are observed in spring and summer. During these seasons, apart from the the Adriatic Sea (especially in the North and along the eastern coast where cumulated fluxes also reach 3 mol $C.m^{-2}$) and some hot spots (Rhodes gyre, Nile plume), DOC exudation seems homogeneous though a north-south gradient is present. Hot spots of DOC exudation are present nearly all year long in the plume of the main rivers.

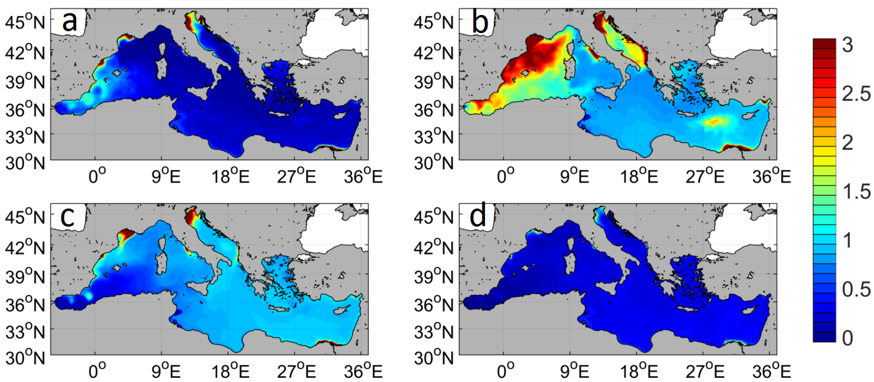

Figure 14. Seasonal variations of mDOC mean 0-100 m exudation cumulated flux by small phytoplankton (in mol C.m^{-2}).

4 Discussion

The dissolved fraction in the organic carbon export is predominant at the scale of the Med Sea

One of the main results of this study is that mDOC export exceeds mPOC export in the whole Mediterranean Basin, with the exception of the Alboran Sea (west of 3°W). This is consistent with the comparisons between POC and DOC exports performed in the Tyrrhennian, North Ionian and Ligurian seas by Copin-Montégut and Avril (1993); Santinelli et al. (2013) or by Lefèvre et al. (1996) who estimated that DOC was the main source of remineralization processes in the aphotic layer. In the Western basin, the ratio of mDOC over mPOC export fluxes ranges between 2 and 5, and is approximately equal to 4 at DyFaMed grid point. Observations at DyFaMed station led to a oDOC export estimation of about 11.9 gC $m^{-2}.y^{-1}$ (Avril, 2002), markedly higher than oPOC export estimations at 200 m which ranged from 1.6 to 2.6 gC $m^{-2}.y^{-1}$ (Miquel et al., 2011) between 2001 and 2005 (by comparison, mPOC is in the range [1.5;3.1] gC $m^{-2}.y^{-1}$ during the same period). In the Northwestern basin, the modeled ratio is about 2 at 100 m and 200 m, while in the same area a modeling study (Herrmann et al., 2014) led to a ratio at 200 m which ranged from 0.9 to 1.8, even though the corresponding export fluxes were higher than in the present study.

The ratio between modeled DOC and POC exports at 100 m ranges from 2 to 8 in the Adriatic Sea. In the same region, a oDOC flux of 15.4 (against 23 for mDOC) gC $m^{-2}.y^{-1}$ was estimated from observations by Santinelli et al. (2013). This is nearly 5 times higher than the measured oPOC export flux under the euphotic zone of 3.3 (against 4.5 for mPOC export at 100 m) gC $m^{-2}.y^{-1}$, which was, however, sampled during a different period (Boldrin et al., 2002).

In the Eastern basin, DOC export is regularly more than 10 times that of POC, due to the very weak POC export and to the high DOC export along the coast and in the open sea. Few observations and estimations are available for this region. In the Northern Ionian Sea, Boldrin et al. (2002) reported low annual oPOC fluxes at 150 m (2.4 gC $m^{-2}.y^{-1}$), which are in the same ordre of magnitude as the simulated annual mPOC fluxes in the same area but for a different period (1.2 gC $m^{-2}.y^{-1}$ and 0.6 gC $m^{-2}.y^{-1}$ at 100 m and 200 m, respectively).

DOC predominance in the OC export flux is first due to the higher DOC gross production fluxes as compared to POC ones, and this still holds if the POC to DOC hydrolysis flux is cancelled (i.e. if the DOC inputs due to POC hydrolysis are not taken into account). At the scale of the Mediterranean Basin, DOC and POC gross production fluxes are respectively equal to 20 10^{12} and 2.7 10^{12} molC.y^{-1}. In the western basin, DOC predominance is still observed although to a lesser extent, with DOC and POC gross production fluxes respectively equal to 8.7 10^{12} and 1.9 10^{12} molC.y^{-1}. In what follows, the reasons of these differences will be further analyzed in the light of the processes associated with DOC and POC production.

POC and DOC exports are characterized by different processes and timing

Strong disparities can be identified between the spatial patterns of the annual DOC and POC export fluxes (figure 5), with rather homogeneous DOC export fluxes across the Mediterranean Basin (though with well identified regions of maximum export that will be analyzed later), contrasting with the high East-West gradient in POC export. This is consistent with in situ measurements of daily POC export across the Mediterranean Sea at 200 m that showed much lower POC export in the Eastern basin than in the Western basin (Moutin and Raimbault, 2002).

Strong differences also exist in the seasonality of DOC and POC export fluxes (Fig. 6 and 7). Hence, over the whole Mediterranean Sea, 88 % of DOC export occurs between November and February, which is coherent with observations at DyFaMed station where 90% of annual DOC export was linked to winter mixing (Avril, 2002). By contrast, POC export is more even throughout the year, and during the same period only 23 % of POC is exported.

In the model, only the detrital compartment (POC) is allowed to sink. The sinking process is therefore the only source of explicit distinction between POC and DOC exports, but it is likely not sufficient to explain the strong aforementioned differences. The main source of difference lies in the biogeochemical processes that fuel or consume POC and DOC pools (see section 2.2. In the model, POC is fueled by the natural mortality of largest organisms (mesozooplankton, diatoms and ciliates) and by the egestion of fecal pellets and sloppy feeding by mesozooplankton. Thus, higher concentrations of large organisms in the Western basin, primarily due to the spring bloom in the liguro-provencal region associated with high primary production rates is the main reason for the higher POC production and export in this basin. Hence, POC export is maximum in spring (i.e. from March to May in figure 7) since it is the period including the maximum and the end of the bloom during which detrital concentrations of large organisms are the highest. Moreover, according to the model, mortality is the main process that fuels the POC pool, far ahead of the egestion and sloppy feeding process. More generally, a strong correlation between annual primary production and POC export has been evidenced at basin scale (spearman's rank correlation coefficient is 0.84), while this is not the case for DOC export (correlation below 0.01).

As shown in the results section, the regions of high POC or DOC export are generally not the same, except for the regions characterized by high primary production rates during the spring bloom, namely the Alboran Sea, the bloom region in the NW Mediterranean Sea and the south of the Adriatic Sea (see also later in the discussion). that combine high productivity and strong physical forcing (i.e. high horizontal velocities associated with high vertical velocities or deep convection). Apart from these regions, the annual DOC export at 100 m is relatively high in almost all the Mediterranean Basin, particularily in autumn and winter, and is the consequence of DOC accumulation in the 0-100 m layer during summer and autumn (Fig. 3) since DOC export indeed takes place when DOC rich surface waters plunge or are mixed with poorer deeper waters. This accumulation of DOC is primarily due to water stratification that results in nutrients exhaustion in the 0-100 m layer. As a result, the pool of DOC in phytoplankton is saturated with newly synthesized organic compounds since photosynthesis (i.e. carbon production), which is not controlled by P-availability, takes place more rapidly than is required to supply the needs of growth (growth being limited by the intracellular quota of P). This results in high DOC exudation by phytoplankton, which is the main source of DOC in the model. The contribution of zooplankton excretion is maximum in spring in the bloom region of the NW Mediterranean, but remains always much lower than that of exudation (results not shown). Similarly, the annual contribution of POC hydrolysis to the DOC production flux is weak (around 10 %). Bacteria are the first consumers of DOC, and the second ingredient for DOC accumulation is therefore a strong nutrient limitation that will highly restrict bacteria growth rate (see Eq. 1). In such a situation, DOC availability may exceed bacteria needs and result in DOC accumulation when DOC production by phytoplankton exceeds DOC uptake by bacteria, and this process is enhanced in hydrodynamical situations where the surface layers are isolated from the deep waters (i.e. stratification period). Such a mechanism of DOC accumulation due to a malfunctioning microbial loop has already been described in Thingstad et al. (1997) and is also the main driver of DOC accumulation in the model. Destratification in autumn leads to a net export as well as an increase of DOC consumption through bacterial activity, driven by nutrient supply from deep water.

DOC accumulation in the light of intracellular quotas

The regions of highest DOC export fluxes correspond to the regions where the highest DOC accumulation occur. It is therefore informative to analyze the occurrence of DOC accumulation in the light of intracellular quotas. Geographical and hydrological considerations are indeed not sufficient for a thorough comprehension of the DOC accumulation pattern at the scale of the Mediterranean Sea.

It has already been said that, according to the model, phytoplankton exudation is the primary source of DOC. High DOC exudation by phytoplankton occurs in nutrient-depleted waters. In such a situation N and/or P phytoplankton nutrient quotas are low and limit growth rate (i.e. the cell division rate). In the model, phytoplankton (and bacteria) specific growth rate (i.e. their cellular division rate) is indeed controlled by the most limiting element among C, N and P (see Eq. (1). In other words, the intracellular quota which is the closest to its minimum value controls the division rate. When P (and/or N) are the most limiting, growth will proceed at low rate and the carbon input due to photosynthesis will rapidly meet phytoplankton needs, thus resulting in an increase in the carbon quota Q_C. Since DOC exudation flux per cell increases with Q_C through a Geider et al. (1998) non linear quota function, DOC exudation flux will highly increase as the quota approaches it maximum value $Q_C^{\max}$. Phytoplankton carbon quota is therefore a good indicator for DOC exudation.

In the oligotrophic Mediterranean Sea, nutrient (and mostly P in the model) depletion is maximum at the end or just after the spring bloom, or under well established conditions of water stratification, thus leading to maximum exudation fluxes (see Fig. 13 and 14). In the rest of the Mediterranean, DOC exudation is maximum in (late) spring and summer, and mainly due to small phytoplankton. The latter is indeed characterized by low phosphorous quotas (see Fig. 10) and high carbon quotas (see Fig. 10).

The driving processes of DOC accumulation are not the same in the Western and the Eastern Mediterranean. In the Western Mediterranean, and especially in the enlarged bloom region, large phytoplankton blooms first and is rapidly P-limited (as early as February) and the same occurs for small phytoplankton though later (i.e. only in spring, see Fig. 10). This is consistent with observations performed in the NW Mediterranean Sea (Gulf of Lions) (Diaz et al., 2001). In this situation, the high phytoplankton exudation fluxes are not only due to phytoplankton carbon quotas that are relatively high (around 50-60%, see the small phytoplankton carbon quota in Fig. 9), resulting in relatively high exudation flux per cell, but to the high phytoplankton abundances. Though exudation fluxes are high in (late) winter due to large phytoplankton (Fig. 13a), the high bacteria P-quotas (Fig. 12a) combined with winter mixing prevents DOC accumulation (Fig. 3a). In spring, and mostly in late spring, bacteria are strongly P-limited (Fig. 12b) since the bloom has rapidly consumed the available nutrients and vertical mixing has stopped. As a result, DOC accumulation starts in this region (3b) and reaches its maximum in summer (3c) during the stratification period since DOC exudation by phytoplankton still proceeds (though at a lower rate) and bacteria are still strongly P-limited (12c). Finally, the end of the stratification in autumn will not only dilute the DOC-rich surface concentrations with DOC-poor deep waters, but allow the P-enrichment of surface waters (see the increase in bacteria Q_P in Fig. 12d).

In the Eastern Mediterranean, DOC accumulation is mainly visible along the southern and eastern coasts. Moreover, it starts later than in the Western Mediterranean (i.e. in summer against spring for the West), and is maximum in autumn. In the model, the Atlantic waters that flow along the coast are less dense (with densities slightly underestimated as compared to in situ measurements (Beuvier, 2011)) and therefore strongly isolated from the rest of the water column. As a result, their nutrients content will be progressiveley consumed and these waters become more and more oligotrophic as they flow along the southern coast of the basin, and always more oligotrophic than the rest of the Eastern basin. In summer and autumn, they can even be considered as ultra-oligotrophic (see the phytoplankton Q_P in Fig. 10c and d). Moreover, they extend over a layer of around 100 m thick in which concentrations are roughly homogeneous. During summer and autumn, bacteria are also strongly P-limited but more and more carbon-rich (see Fig. 11) since phytoplancton exudation still proceeds (though at extremely low rates in autumn). Moreover, the vertical mixing that starts in autumn is not sufficiently deep to reach the nutrient-rich waters since the MLD is shallower than the bottom of these Atlantic waters. In addition, since DOC concentration is high over the whole layer, DOC surface concentration are not diluted by the mixing. As a result, accumulation still proceeds until winter where higher MLD will allow the P-enrichment in surface waters and dilute surface DOC concentrations as well.

Furthermore, DOC concentrations (as well as DOC annual export flux though this is more difficult to see in Fig.5) are negligeable throughout the year in some well identified regions, namely the two cyclonic structures in the Tyrrhenian Sea, the south of the Adriatic Sea (excluding the coastal zones), and the region of the Rhodes Gyre in the Levantin basin. All these structures are characterized by regular input of nutrients from deep waters, resulting in an absence of strong P-limitation in bacteria. In such conditions, bacteria carbon quota is rather low and DOC accumulation and export can not occur.

Finally, the strong link between low phosphate availability in the upper surface water of the Mediterranean Sea and DOC accumulation due to nutrient limitation of bacterial production that is evidenced in this modeling study is consistent with previous in situ (Moutin et al., 2002; Van Wambeke et al., 2002) and modeling (Thingstad et al., 1997) studies and is shown to apply at the whole Mediterranean Basin, with the exception of the aforementioned specific regions.

Discussion on results robustness

Though difficult to achieve in a rigorous way, the robustness of our main results will be discussed in what follows. As shown in section (2.2), the model includes many DOC and POC production and consumption processes. A sensitivity study on all the parameters they involve is obviously impossible to achieve, though some attempts towards this goal have already been done in Baklouti et al. (2006b). Moreover, accounting for the fact that most of the parameters used have a physiological meaning (including cell size considerations), and constitute a coherent set that remains unchanged for the different studies undertaken with Eco3M-MED (even outside the Mediterranean), their values are rather reliable. However, POC to DOC hydrolysis rate and the sinking velocity are not physiological parameters and their impact on the results will be discussed later.

The comparison of DOC stocks with the few available results (see section A4 in Appendix) showed that, though the modeled DOC vertical profiles were quite different (but in the same order of magnitude) than the measured ones, modeled and measured integrated DOC stocks over the 0-100 m layer showed much better agreement. Furthermore, when compared with the few available measurements to in situ estimations of DOC export from the DyFaMed station (Avril, 2002), and the Adriatic and the Tyrrhenian seas (Santinelli et al., 2013), the model always provides higher DOC export values. These differences in DOC export may be partly attributable to the model failures discussed in section (A4) but, as already mentioned, high uncertainties are also associated with in situ estimations. Hence, according to (Santinelli et al., 2013), DOC export computations from stock differences below the euphotic layer probably underestimate the real flux. This is also the conclusion we came to by using model outputs to compute export fluxes with our method and with the in situ method. If we assume, however, that the different in situ evaluations are consistent with each other, it appears that the highest DOC export occurs in the Adriatic Sea, followed by DyFaMed station

(Ligurian Sea) and then by the Tyrrhenian Sea, and the same order can be inferred from the model outputs.

Two parameters are essential in POC export, namely POC to DOC hydrolysis rate and the sinking velocity. In the model, the hydrolysis rate of POC to DOC is modulated by the bacteria carbon quota. In substance, the higher the carbon quota, the more the hydrolysis rate decreases and eventually becomes 0 when the bacteria carbon quota is maximum. Moreover, the influence of the hydrolysis rate is all the more important that the sinking velocity is low. When sinking velocity is high, POC will indeed be quickly exported before being hydrolyzed. In the present model, there is a single detrital compartment which includes small and large particles. The sinking velocity has been fixed to an intermediate value of 2 m d^{-1} which may reflect an underestimation of the actual mean value though this is difficult to verify. In several other models (e.g. Lévy et al., 1998; Lacroix and Gregoire, 2002; Herrmann and Somot, 2008), two detrital compartments are used, thus allowing to differenciate between low and high sinking rates of detrital particules. However, in these models, the large detrital compartment is only fueled by mesozooplankton fecal pellets (Lévy et al., 1998), by micro and mesozooplankton fecal pellets (Herrmann and Somot, 2008), or by the mesozooplankton mortality and fecal pellets (Lacroix and Gregoire, 2002), and these fluxes, except the mesozooplankton mortality, are likely weak in our model compared to the other POC sources (which is dominated by the mortality of the largest organisms). Moreover, our model includes more POC sources since ciliates mortality and sloppy feeding by mesozooplankton also fuel the POC pool. Finally, the hydrolyzis rate that has been used (i.e. 0.03 d^{-1}) is rather low compared to the aforementioned modeling papers, and may partly compensate the likely underestimated sinking rate. Apart from these two parameters, it has been seen that the model underestimates Chl concentrations at the DCM (mainly due to a lack of large phytoplankton) and this may also lead to an underestimation of POC export. However, the 0-100 m mIPP values are consistent with oIPP thereby suggesting that this DCM underestimation has only a limited impact on carbon production. Overall, the annual POC export flux at 100 m provided by the model is around 8$\%$ of the annual primary production, a value that is coherent with in situ estimations.

Between 100 m and 200 m however, the mean bacteria carbon quota is lower since POC hydrolysis and bacteria and heterotrophic nanoflagellates mortalities are the only sources of DOC, resulting in higher hydrolysis rates and in lower POC export at 200 m. Looking at the vertical attenuation of POC fluxes, it is common to use a power law expressed as $F(z) = F(z = z_0) * (\frac{z}{z_0})^{-b}$, where F(z) is the depth-dependent POC flux and b a positive coefficient whose values may vary according to the location or the period. In regions of significant export, b values inferred from the model outputs fluctuate between 0.9 in the Provencal sub-basin and 2.3 for the Algerian basin. Values of b derived from observations tend to be lower: 0.92 and 1.0 for the Western and Eastern moorings, respectively (Gogou et al., 2014), or 0.75 in the Alboran Sea (Zúñiga et al., 2007). This again suggests that the attenuation of POC export flux between 100 m and 200 m is too great in the model. Furthermore, when compared to the few available data of POC export fluxes, the model always underestimates the export flux in the Eastern basin. However, all the in situ estimations we could find in literature were done at 150 m or 200 m depth, that means in the 100-200 m layer where the modeled POC export is more likely underestimated. In summary, all this suggests that the underestimation of POC export fluxes is more likely effective at 200 m than at 100 m depth though the comparison at DyFaMed station shows that the mean mPOC export (5.6 $gC.m^{-2}.y^{-1}$ and 2.2 $gC.m^{-2}.y^{-1}$ at 100 m and 200 m respectively) is in the range of the measured one at 200 m (i.e. [1.6;2.6] $gC.m^{-2}.y^{-1}$ (Miquel et al., 2011)). Finally, it is very unlikely that the aforementioned uncertainties could put in question the predominance of DOC in the OC export in the Eastern basin. This conclusion also applies in the Western basin (though will less certainty), all the more that in situ measurements allow to draw the same conclusion (Copin-Montégut and Avril, 1993; Avril, 2002; Miquel et al., 2011).

Model accuracy

Due to the high complexity of the biogeochemical model and the scarcity of data, the assessment of the model's representativeness at the scale of the Mediterranean Sea is a complex task.

This work, however, aims at performing comparisons on several modeled variables, at different time and space scales when in situ measurements were available. If the model and observations are mostly in agreement, some discrepancies have been identified that will now be discussed. In the Adriatic Sea and along the Algerian coast, observed chlorophyll concentrations and primary production patterns are not well reproduced, which may be partly due to the hydrodynamic simulation that does not identify the actual physical structures well and slightly underestimate the Algerian current intensity (Soto-Navarro et al., 2014). In the most oligotrophic regions, (Levantine, Ionian and Tyrrhenian Seas), modeled chlorophyll does not match the seasonal pattern identified with satellite data, since the higher concentrations modeled are in summer instead of spring. This shortcoming can be largely relativized by the fact that the mean surface chlorophyll in summer equals 0.06 $\mu g\ l^{-1}$ and does not differ significantly from the satellite measurement (0.04 $\mu g\ l^{-1}$). Furthermore, surface chlorophyll in the model is estimated as the mean over the first 10 m of the water column, and therefore includes part of the chlorophyll gradient towards the DCM. Finally, the summer functioning of the surface layer is well reproduced by the model : small phytoplankton are largely dominant and maintain their activity thanks to the microbial loop. Conversely, in regions associated with high nutrient inputs (Ligurian Sea, Alboran Sea) the temporal evolution of surface chlorophyll is reproduced but concentrations are overestimated during the bloom (Fig. 19 b and f).

Nutrient concentrations are slightly lower in the model than in observations in almost every vertical layer. This can be attributed to an underestimation of initial nutrient stocks at depth. The model tends to overestimate surface nitrate concentrations during periods of intense stratification (see paragraph 3.1.1). This may be related to an overestimation of nitrification processes, and/or an underestimation of detrital organic matter sinking. Nitrification is, indeed, a linear function with a fixed parameter and does not take into account potential dependancies of the process (e.g. Paulmier et al., 2009).

Looking at the vertical attenuation of POC fluxes, it is common to use a power law expressed as $F(z) = F(z = z_0) * (\frac{z}{z_0})^{-b}$, where F(z) is the depth-dependent POC flux and b a positive coefficient whose values may vary according to the location or the period. In regions of significant export, b values inferred from the model outputs fluctuate between 0.9 in the Provencal sub-basin and 2.3 for the Algerian basin. Values of b derived from observations tend to be lower: 0.92 and 1.0 for the Western and Eastern moorings, respectively (Gogou et al., 2014), or 0.75 in the Alboran Sea (Zúñiga et al., 2007). This suggests that the attenuation of POC export flux is too great in the model. Two explanations can be put forward for this: (i) first, the model does not differentiate between small and large detrital particles, and the mean sinking velocity used for simulation may be underestimated, and (ii) second, the model may overestimate POM hydrolysis. As a consequence, the nitrate stock remains too great in the surface water. Finally, the contribution of large phytoplankton (which fuels the POM compartment) to primary production may be underestimated, as suggested by the comparison with DyFaMed data (see Sect. 3.1.2) and with findings from the BOUM cruise in the Eastern basin (Crombet et al., 2011) and this could be due to an underestimation of phosphate stocks, and/or an overestimation of light attenuation. Thus, though perfectible, this work does provide unique insight into the spatial and temporal variabilities of organic carbon export in the Mediterranean Sea. Seasonal maps of DOC and POC exports at basin scale are inexistent in both modeling and observational studies. Due to the large uncertainties associated with methodologies dedicated to estimating carbon export from in situ observations, the evaluation of export maps from in situ data is challenging. For particulate organic carbon, trap efficiency is, indeed, regularly questioned in the literature (e.g. Ducklow et al., 2001), whereas the different methods used to estimate DOC export are indirect methods based on strong hypotheses.

Predominance of dissolved fraction in the organic carbon export

Model results show a preponderance of DOC in the total organic export below both 100 m and 200 m depths in most regions of the Mediterranean Sea. This is consistent with the comparisons between POC and DOC exports performed by Santinelli et al. (2013); Copin-Montégut and Avril (1993) or Lefèvre et al. (1996) who estimated that DOC was the main source of remineralization processes in the aphotic layer. One of the main results of this study is that DOC export exceeds POC export in the whole Mediterranean Basin, with the exception of in the Alboran Sea (west of 3°W). In the Western basin, the ratio of DOC over POC export fluxes is comprised between 2 and 5, and is approximately equal to 4 at DyFaMed grid point, where DOC (POC) export at 100 m is 23.5 (5.6) gC $m^{-2}.y^{-1}$. Observations at DyFaMed station led to a DOC export estimation of 11.9 gC $m^{-2}.y^{-1}$ (Avril, 2002), markedly higher than POC export estimations at 200 m which ranged from 1.2 to 7 gC $m^{-2}.y^{-1}$ (Miquel et al., 2011; Copin-Montégut and Avril, 1993). In the Northwestern basin, the modeled ratio is about 2 at 100 m and 200 m, while in the same area a modeling study (Herrmann et al., 2014) led to a ratio at 200 m which ranged from 0.9 to 1.8, even though the corresponding export fluxes were higher than in the present study.

The ratio between modeled DOC and POC exports at 100 m ranges from 2 to 8 in the Adriatic Sea, with a median value of 5.2. In the same region, a DOC flux of 15.4 gC $m^{-2}.y^{-1}$ was estimated from observations by Santinelli et al. (2013). This is nearly 5 times higher than the measured POC export flux of 3.3 gC $m^{-2}.y^{-1}$, which was, however, sampled during a different period (Boldrin et al., 2002).

In the Eastern basin, DOC export is regularlty more than 10 times that of POC, due to the very weak POC export and to the high DOC export along the coast and in the open sea. Few observations and estimations are available for this region. In the Northern Ionian Sea, Boldrin et al. (2002) reported low annual POC fluxes at 150 m (2.4 gC $m^{-2}.y^{-1}$), which are slightly higher than the simulated annual POC fluxes in the same area (1.2 gC $m^{-2}.y^{-1}$ and 0.6 gC $m^{-2}.y^{-1}$ at 100 m and 200 m, respectively). In situ measurements of daily POC export across the Mediterranean Sea at 200 m showed strong differences, with lower POC export in the Eastern basin than in the Western basin (Moutin and Raimbault, 2002). When compared with the few available measurements of DOC export from the DyFaMed station, the Adriatic Sea, and the Tyrrhenian Sea, the model always provides higher DOC export values. These differences in DOC export may be partly attributable to model failures, but, as already mentioned, high uncertainties are also associated with in situ estimations. For example, DOC export computations from stock differences below the euphotic layer probably underestimate the real flux (Santinelli et al., 2013). If we assume, however, that the different in situ evaluations are consistent with each other, it appears that the highest DOC export occurs in the Adriatic Sea, followed by DyFaMed station (Ligurian Sea) and then by the Tyrhhenian Sea, and the same order can be inferred from the model outputs.

The consistency demonstrated between in situ data of organic carbon export fluxes and the corresponding fluxes provided by the present model has several implications. First, it strengthens the reliability of our results and , in particular, highlights the major role of the dissolved fraction of total organic carbon export below the euphotic layer. In the context of climate change, this has a more far-reaching implication, since the enhanced stratification that should accompany an increase in temperature is expected to result in an increase of DOC production (Santinelli et al., 2013; Lazzari et al., 2013), and thereby further increase the importance of DOC in the biological carbon pump.

Relationships between POC and DOC export

Export of POC and DOC fluxes are associated with different processes occurring at different times of the year. As a result, over the whole Mediterranean Sea, 88 % of DOC export occurs between November and February, which is coherent with observations at DyFaMed station where 90% of annual DOC export was linked to winter mixing (Avril, 2002). By contrast, POC export is more even throughout the year, and during the same period (i.e. from November to February) only 23 % of POC is exported. At DyFaMed station, both observed and modeled seasonal signals are dominated by high POC fluxes connected to blooms of large organisms, with a maximum in February-March for in situ data (Miquel et al., 2011), and in April for the model. Finally, a strong correlation between annual primary production and POC export can be evidenced (spearman's rank correlation coefficient is 0.84), while this is not the case for DOC export (correlation below 0.01). Generally, the spatial correlation between POC and DOC fluxes is weak. Regions of high POC (DOC) export (see contours in Fig. 5) generally do not match. For example, the Alboran Sea is characterized by high POC export fluxes as well as by relatively low DOC export fluxes. The only areas associated with both high POC and DOC exports are the Algerian coast, the Adriatic coast, the regions of deep convection and a band east of the Balearic Islands. Each of these regions is associated with considerable productivity and high physical variability (high horizontal velocities and deep convection).

Spatial and time variability of DOC export in the light of processes

Some differences in the mechanisms of DOC export can be identified between regions. For example, in the center of the Ionian basin, DOC stock in the first 100 m increases from May to November as DOC production processes (mainly exudation by P-limited phytoplankton during summer) dominates DOC consumption (bacterial activity is limited by nutrients). Destratification in autumn leads to a net export as well as an increase of DOC consumption through bacterial activity, driven by nutrient supply from deep water. During this period, primary production is weak. In the North Western Mediterranean, which is characterized by deep convection events in winter, two distinct periods can be identified in the process of DOC export. During the first period, DOC stocks that accumulated during summer are progressively exported as soon as the water column is destratified (November-December), following a similar process to that already mentioned for the Ionian basin : during this period, the total DOC stock decreases. The second period occurs in March, when primary production begins to increase while the mixing layer is still deep. In this case, DOC export is concomitant with its production via DOC exudation by phytoplankton during the bloom. DOC export patterns along the Algerian coast and the continental slopes are different, as they occur all year long with particularly high fluxes between October and May. In these regions, DOC stocks above 100 m remain high throughout the year, which is also diagnosed by the rare occurrence of C-limitation of bacteria at 100 m depth (see Fig. **??**). This DOC accumulation is mainly due to lateral advection and exudation by small phytoplankton. In these regions, carbon export fluxes are much higher than elsewhere and are mainly associated with downwelling processes.

5 Conclusions

A 14-year simulation combining a high resolution physical model (NEMO-MED12) and a biogeochemical model (Eco3M-MED) has been built to study carbon organic production and fate at the scale of the Mediterranean Sea.

The first part of this work A preliminary work presented in Appendix focused on the model skill assessment through an extensive comparison of different model outputs (i.e. chlorophyll, but also nutrients, primary production and DOC profiles) with available data at various time and space scales Corresponding results show, in general, a globally satisfying representation allowed to verify the model ability in representing the main features of the biogeochemical functioning of the Mediterranean Sea. In the second part of this work results section, carbon export fluxes are investigated. Previous estimations of DOC export in the Mediterranean Sea were restricted to specific regions of the Mediterranean Sea (e.g. the Ligurian, Adriatic, Tyrrhenian Seas). We here propose the first basin Mediterranean-scale view of annual DOC and POC export fluxes, as well as an analysis of their spatial and seasonal variations.

A major result The two major results of this modeling study concerns lye in (i) the predominance of the Eastern basin in OC export (with nearly 60 % of the OC export occuring in the Eastern basin), and (ii) in the crucial role of the dissolved fraction in the total organic carbon export. At the Mediterranean scale, DOC export represents about four fifths of total organic carbon fluxes, thereby attesting to its major role in the carbon cycle and the biological pump in the Mediterranean Sea. Regions of non C-limited bacteria are preferential for DOC export, and this is particularly the case for continental slopes and the south Ionian Sea. The concept of malfunctioning microbial loop (Thingstad et al., 1997) due to high P-limitation of both phytoplankton and bacteria, and leading to high DOC exudation fluxes beyond bacterial needs also applies in the present study though it is generalized to the whole Mediterranean Basin, except some specific P-rich regions (see results and discussion). Export in the Eastern basin is markedly high despite its lower productivity compared to the Western basin. By contrast, POC export is closely associated with regions characterized by high productivity. As a consequence, total carbon export in the Eastern basin is considerably higher than expected as regards its low primary productivity. , and barely lower than that of the Western basin. Results also show high spatial variability in organic carbon fluxes and a temporal uncoupling between POC and DOC exports. This is attributable to the differences in the processes involved in the production and export of POC and DOC.

Further comparisons with observations are clearly necessary to confirm these results, which emphasizes the need for in situ temporal monitoring to properly quantify organic carbon export. This study also identifies the need to examine the microbial food web in detail in order to further investigate the carbon cycle in the Mediterranean Sea. Impacts of potential limitations of the different planktonal functional type could also be adressed in a future work. A thorough analysis of the biogeochemical functionning of the Mediterranean Sea, in the light of the intracellular quotas should also be conducted in future work. Finally, Furthermore, the implementation of an explicit inorganic carbon compartment in the biogeochemical model would close the carbon budget and help in the full characterization of the biological pump.

In conclusion, the strong link between low phosphate availability in the upper surface water of the Mediterranean Sea and DOC accumulation due to nutrient limitation of bacterial production already identified by previous modeling (Thingstad et al., 1997) and in situ (Moutin et al., 2002; Van Wambeke et al., 2002) studies is strenghtened by this modeling study which may therefore be of interest for other oceanic regions. Upper waters low phosphate availabilities have indeed been identified in other oceanic regions like the Sargasso Sea (Wu et al., 2000), the North Pacific or the South West Pacific (Van Den Broeck et al., 2004) and high DOC accumulation were also reported in some of these areas (Carlson et al., 1994). This work may therefore be of interest for these oceanic regions. Finally, in the context of climate change, the enhanced stratification and the likely geographical extension of low phosphate availability in upper waters (Karl et al., 1997; Moutin et al., 2008) is expected to result in an increase in DOC production (Santinelli et al., 2013; Lazzari et al., 2013), and thereby further increase the importance of DOC in the biological carbon pump.

Acknowledgements. Authors are grateful to the different supports that funded this work. This includes the PACA French region (who funded the phD thesis of A. Guyennon), the Mercator Ocean group (who funded the SiMED project that provided an efficient framework for this work), the MED-ICCBIO project (funded by the *Groupement d' Intérêt Scientifique* "Climat, Environnement et Société"), and the OT-MED Labex. This work is a contribution to the MerMEx and the OT-MED programs and it was granted access to the HPC resources of IDRIS (Institut du Développement et des Ressources en Informatique Scientifique) of the Centre National de la Recherche Scientifique (CNRS). The DYFAMED time series have been provided by the Oceanological Observatory (CNRS-UPMC) of Villefranche-sur-Mer (L.Coppola). This project is funded by CNRS-INSU and ALLENVI through the MOOSE observing network. The satellite data used in this is study are MyOcean Products. Authors are also grateful to Jean-Michel André for his help and relevant advices, and to L. Coppola for his very efficient assistance to obtain in situ data from DyFaMed station.

References

Alekseenko, E., Raybaud, V., Espinasse, B., Carlotti, F., Queguiner, B., Thouvenin, B., Garreau, P., and Baklouti, M.: Seasonal dynamics and stoichiometry of the planktonic community in the NW Mediterranean Sea: a 3D modeling approach, Ocean Dynamics, 64, 179–207, 2014.

Antoine, D., Morel, A., and André, J.: Algal pigment distribution and primary production in the eastern Mediterranean as derived from coastal zone color scanner observations, Journal of Geophysical Research, 100, 16 193–16, 1995.

Avril, B.: DOC dynamics in the northwestern Mediterranean Sea (DYFAMED site), Deep Sea Research Part II: Topical Studies in Oceanography, 49, 2163–2182, 2002.

Baklouti, M., Diaz, F., Pinazo, C., Faure, V., and Quéguiner, B.: Investigation of mechanistic formulations depicting phytoplancton dynamics for models of marine pelagic ecosystems and description of a new model, Progress in Oceanography, 71, 1–33, 2006a.

Baklouti, M., Faure, V., Pawlowski, L., and Sciandra, A.: Investigation and sensitivity analysis of a mechanistic phytoplankton model implemented in a new modular numerical tool (Eco3M) dedicated to biogeochemical modelling, Progress in Oceanography, 71(1), 34–58, 2006b.

Baklouti, M., Chevalier, C., Bouvy, M., Corbin, D., Pagano, M., Troussellier, M., and Arfi, R.: A study of plankton dynamics under osmotic stress in the Senegal River Estuary, West Africa, using a 3D mechanistic model, Ecological Modelling, 222, 2704–2721, 2011.

Baretta, J., Ebenhoh, W., and Ruardij, P.: The European Regional Seas Ecosystem Model, a complex marine ecosystem model, J. Sea Res., 33, 233–246, 1995.

Béranger, K., Mortier, L., and Crépon, M.: Seasonal variability of water transport through the Straits of Gibraltar, Sicily and Corsica, derived from a high-resolution model of the Mediterranean circulation, Progress in Oceanography, 66, 341–364, 2005.

Beuvier, J.: Modélisation de la variabilité climatique de la circulation et des masses d'eau en mer Méditerranée: impact des échanges océan-atmosphére, Ph.D. thesis, Ecole Polytechnique, 2011.

Beuvier, J., Sevault, F., Herrmann, M., Kontoyiannis, H., Ludwig, W., Rixen, M., Stanev, E., Béranger, K., and Somot, S.: Modeling the Mediterranean Sea interannual variability during 1961–2000: focus on the Eastern Mediterranean Transient, Journal of Geophysical Research: Oceans (1978–2012), 115, doi:10.1029/2009JC005950, 2010.

Beuvier, J., Béranger, K., Brossier, C., Somot, S., Sevault, F., Drillet, Y., Bourdallé-Badief, R., Ferry, N., Lyard, F., et al.: Spreading of the Western Mediterranean Deep Water after winter 2005: Time scales and deep cyclone transport., Journal of Geophysical Research, 117, doi:10.1029/2011JC007679, 2012a.

Beuvier, J., Lebeaupin Brossier, C., Béranger, K., Arsouze, T., Bourdallé-Badie, R., C., D., Drillet, Y., Drobinski, P., Lyard, F., Ferry, N., Sevault, F., and Somot, S.: Oceanic component for the modeling of the regional Mediterranean Eart System., Mercator Ocean Quarterly Newsletter, 46, 60–66, 2012b.

Boldrin, A., Miserocchi, S., Rabitti, S., Turchetto, M., Balboni, V., and Socal, G.: Particulate matter in the southern Adriatic and Ionian Sea: characterisation and downward fluxes, Journal of Marine Systems, 33, 389–410, 2002.

Bopp, L., Monfray, P., Aumont, O., Dufresne, J., Le Treut, H., Madec, G., Terray, L., and Orr, J.: Potential climate change on marine export production, Global Biogeochemical Cycles, 15, 81–99, 2001.

Bosc, E., Bricaud, A., and Antoine, D.: Seasonal and interannual variability in algal biomass and primary production in the Mediterranean Sea, as derived from 4 years of SeaWiFS observations, Global Biogeochemical Cycles, 18, GB1005, doi:10.1029/2003GB002034, 2004.

Buesseler, K.: Do upper-ocean sediment traps provide an accurate record of particle flux ?, Nature, 353, 420–423, 1991.

Carlson, C., Ducklow, H., and Michaels, A.: Annual flux of dissolved organic carbon from the euphotic zone in the northwestern Sargasso Sea, Nature, 371, 405–408, 1994.

Claustre, H., Morel, A., Hooker, S., Babin, M., Antoine, D., Oubelkheir, K., Bricaud, A., Leblanc, K., Queguiner, B., and Maritorena, S.: Is desert dust making oligotrophic waters greener ?, Geophysical Research Letters, 29, 107–1–107–4, 2002.

Copin-Montégut, G. and Avril, B.: Vertical distribution and temporal variation of dissolved organic carbon in the North-Western Mediterranean Sea, Deep Sea Research Part I: Oceanographic Research Papers, 40, 1963–1972, 1993.

Crise, A., Crispi, G., and Mauri, E.: A seasonal three-dimensional study of the nitrogen cycle in the Mediterranean Sea: Part I. Model implementation and numerical results, Journal of Marine Systems, 18, 287–312, 1998.

Crispi, G., Crise, A., and Solidoro, C.: Three-dimensional oligotrophic ecosystem models driven by physical forcing: the Mediterranean Sea case, Environmental Modelling Software, 13, 483–490, 1998.

Crombet, Y., Leblanc, K., Queguiner, B., Moutin, T., Rimmelin, P., Ras, J., Claustre, H., Leblond, N., Oriol, L., and Pujo-Pay, M.: Deep silicon maxima in the stratified oligotrophic Mediterranean Sea, Biogeosciences, 8, 459–475, 2011.

Diaz, F., Raimbault, P., Boudjellal, B., Garcia, N., and Moutin, T.: Early spring phosphorus limitation of primary productivity in a NW Mediterranean coastal zone (Gulf of Lions), Marine Ecology Progress Series, 211, 51–62, 2001.

D'Ortenzio, F. and Ribera d'Alcalà, M.: On the trophic regimes of the Mediterranean Sea: a satellite analysis, Biogeosciences, 6, 139–148, 2009.

D'Ortenzio, F., Marullo, S., Ragni, M., Ribera d'Alcalà, M., and Santoleri, R.: Validation of empirical SeaWiFS algorithms for chlorophyll-a retrieval in the Mediterranean Sea: A case study for oligotrophic seas, Remote Sensing of Environment, 82, 79–94, 2002.

Droop, M.: Vitamin B12 and marine ecology. IV. The kinetics of uptake, growth and inhibition in Monochrysis lutheri, J. Mari. Biol. Assoc. UK, 48, 689–733, 1968.

Ducklow, H., Steinberg, D., and Buesseler, K.: Upper ocean carbon export and the biological pump, Oceanography-Washington DC-Oceanography Society, 14, 50–58, 2001.

Eppley, R. and Peterson, B.: Particulate organic matter flux and planktonic new production in the deep ocean, Nature, 282, 677–680, 1979.

Fasham, M., Flynn, K., Pondaven, P., Anderson, T., and Boyd, P.: Development of a robust marine ecosystem model to predict the role of iron in biogeochemical cycles: A comparison of results for iron-replete and iron-limited areas, and the SOIREE iron-enrichment experiment, Deep Sea Research Part I: Oceanographic Research Papers, 53, 333–366, 2006.

Garcia, H. E., Locarnini, R., Boyer, T., and Antonov, J.: World Ocean Atlas 2005. Vol. 4, Nutrients (phosphate, nitrate, silicate), 2006.

Geider, R., MacIntyre, H., and Kana, T.: A dynamic regulatory model of phytoplankton acclimation to light, nutrients, and temperature, Limnology and Oceanography, 43, 679–694, 1998.

Gogou, A., Sanchez-Vidal, A., Durrieu de Madron, X., Stavrakakis, S., Calafat, A. M., Stabholz, M., Psarra, S., Canals, M., Heussner, S., Stavrakaki, I., et al.: Carbon flux to the deep in three open sites of the Southern European Seas (SES), Journal of Marine Systems, 129, 224–233, 2014.

Gómez, F.: The role of the exchanges through the Strait of Gibraltar on the budget of elements in the Western Mediterranean Sea: consequences of human-induced modifications, Marine Pollution Bulletin, 46, 685–694, 2003.

Hansell, D. and Carlson, C.: Marine Dissolved Organic Matter and the Carbon Cycle, Oceanography, 14, 685–716, 2001.

Hansell, D., Carlson, C., and Suzuki, Y.: Dissolved organic carbon export with North Pacific Intermediate Water formation, Global Biogeochemical Cycles, 16, 7–1–7–8, 2002.

Hansell, D., Repeta, D., Carlson, C., and Schlitzer, R.: Dissolved organic matter in the ocean: A controversy stimulates new insights, Oceanography, 22, 202–211, 2009.

Herrmann, M. and Somot, S.: Relevance of ERA40 dynamical downscaling for modeling deep convection in the Mediterranean Sea, Geophysical Research Letters, 35, doi:10.1029/2007GL032442, 2008.

Herrmann, M., Diaz, F., Estournel, C., Marsaleix, P., and Ulses, C.: Impact of atmospheric and oceanic interannual variability on the Northwestern Mediterranean Sea pelagic planktonic ecosystem and associated carbon cycle, Journal of Geophysical Research: Oceans, 118, 1–22, 2014.

Holling, C.: Some characteristics of simple types of predation and parsitism, The Candian Entomologist, 91, 385–398, 1959.

Karl, D. M., Letelier, R. M., Tupas, L., Dore, J., Christian, J., and Hebel, D.: The role of nitrogen fixation in biogeochemical cycling in the subtropical North Pacific Ocean, Nature, 387, 533–538, 1997.

Kooijman, S. A. L. M.: Dynamic Energy and Mass Budgets in Biological Systems, Cambridge University Press, Cambridge, UK, 2000.

Lacroix, G. and Gregoire, M.: Revisited ecosystem model (MODECOGeL) of the Ligurian Sea: seasonal and interannual variability due to atmospheric forcing, Journal of Marine Systems, 37, 229–258, 2002.

Lavigne, H., D'Ortenzio, F., Migon, C., Claustre, H., Testor, P., d'Alcalà, M., Lavezza, R., Houpert, L., and Prieur, L.: Enhancing the comprehension of mixed layer depth control on the Mediterranean phytoplankton phenology, Journal of Geophysical Research: Oceans, 118, 3416–3430, 2013.

Lazzari, P., Solidoro, C., Ibello, V., Salon, S., Teruzzi, A., Béranger, K., Colella, S., and Crise, A.: Seasonal and inter-annual variability of plankton chlorophyll and primary production in the Mediterranean Sea: a modelling approach, Biogeosciences, 8, 5379–5422, 2012.

Lazzari, P., Mattia, G., Solidoro, C., Salon, S., Crise, A., Zavatarelli, M., Oddo, P., and Vichi, M.: The impacts of climate change and environmental management policies on the trophic regimes in the Mediterranean Sea: Scenario analyses, Journal of Marine Systems, 2013.

Le Quéré, C., Takahashi, T., Buitenhuis, E., Rödenbeck, C., and Sutherland, S.: Impact of climate change and variability on the global oceanic sink of CO2, Global Biogeochemical Cycles, 24, 2016–2040, 2010.

Le Quéré, C. L., Harrison, S., P., C., Buitenhuis, E., Aumont, O., Bopp, L., Claustre, H., Cotrim Da Cunha, L., Geider, R., Giraud, X., et al.: Ecosystem dynamics based on plankton functional types for global ocean biogeochemistry models, Global Change Biology, 11, 2016–2040, 2005.

Lebeaupin Brossier, C., Béranger, K., Deltel, C., and Drobinski, P.: The Mediterranean response to different space–time resolution atmospheric forcings using perpetual mode sensitivity simulations, Ocean Modelling, 36, 1–25, 2011.

Leblanc, K., Quéguiner, B., Garcia, N., Rimmelin, P., and Raimbault, P.: Silicon cycle in the NW Mediterranean Sea: seasonal study of a coastal oligotrophic site, Oceanologica Acta, 26, 339–355, 2003.

Lefèvre, D., Denis, M., Lambert, C., and Miquel, J.: Is DOC the main source of organic matter remineraliztion in the ocean water column ?, Journal of Marine Systems, 7, 281–291, 1996.

Lévy, M., Mémery, L., and André, J.: Simulation of primary production and export fluxes in the Northwestern Mediterranean Sea, Journal of Marine Research, 56, 197–238, 1998.

Ludwig, W.: Continental erosion and river transport of organic carbon to the world's Oceans, Ph.D. thesis, Université Louis Pasteur de Strasbourg, 1996.

Ludwig, W., Dumont, E., Meybeck, M., and Heussner, S.: River discharges of water and nutrients to the Mediterranean and Black Sea: Major drivers for ecosystem changes during past and future decades?, Progress in Oceanography, 80, 199–217, 2009.

Macías, D., Stips, A., and Garcia-Gorriz, E.: The relevance of deep chlorophyll maximum in the open Mediterranean Sea evaluated through 3D hydrodynamic-biogeochemical coupled simulations, Ecological Modelling, 281, 26–37, 2014.

Madec, G. and The-NEMO-Team: NEMO ocean engine, Note du pole de modélisation de l'IPSL, 27, 1228–1619, 2008.

Maier-Reimer, E., Mikolajewicz, U., and Winguth, A.: Future ocean uptake of CO2: interaction between ocean circulation and biology, Climate Dynamics, 12, 711–722, 1996.

Marshall, J. and Schott, F.: Open-ocean convection: Observations, theory, and models, Reviews of Geophysics, 37, 1–64, 1999.

Marty, J. and Chiavérini, J.: Seasonal and interannual variations in phytoplankton production at DYFAMED time-series station, northwestern Mediterranean Sea, Deep Sea Research Part II: Topical Studies in Oceanography, 49, 2017–2030, 2002.

Marty, J. and Chiavérini, J.: Hydrological changes in the Ligurian Sea (NW Mediterranean, DYFAMED site) during 1995–2007 and biogeochemical consequences, Biogeosciences, 7, 2117–2128, 2010.

Marty, J., Chiavérini, J., Pizay, M., and Avril, B.: Seasonal and interannual dynamics of nutrients and phytoplankton pigments in the western Mediterranean Sea at the DYFAMED time-series station (1991–1999), Deep Sea Research Part II: Topical Studies in Oceanography, 49, 1965–1985, 2002.

Marty, J.-C., Garcia, N., and Raimbault, P.: Phytoplankton dynamics and primary production under late summer conditions in the NW Mediterranean Sea, Deep Sea Research Part I, 55, 1131–1149, 2008.

Mattia, G., Zavatarelli, M., Vichi, M., and Oddo, P.: The Eastern Mediterranean Sea biogeochemical dynamics in the 1990s: A numerical study, Journal of Geophysical Research: Oceans, 118, 2231–2248, 2013.

Mauriac, R., Moutin, T., and Baklouti, M.: Accumulation of DOC in Low Phosphate Low Chlorophyll (LPLC) area: is it related to higher production under high N: P ratio?, Biogeosciences, 8, 933–950, 2011.

Meador, T., Gogou, A., Spyres, G., Herndl, G., Krasakopoulou, E., Psarra, S., Yokokawa, T., De Corte, D., Zervakis, V., and Repeta, D.: Biogeochemical relationships between ultrafiltered dissolved organic matter and picoplankton activity in the Eastern Mediterranean Sea, Deep Sea Research Part II: Topical Studies in Oceanography, 57, 1460–1477, 2010.

MERMEX-group: Marine ecosystems' responses to climatic and anthropogenic forcings in the Mediterranean, Progress in Oceanography, 91, 97–166, 2011.

Millot, C. and Taupier-Letage, I.: Circulation in the Mediterranean sea, in: The Mediterranean Sea, pp. 29–66, Springer, 2005.

Miquel, J., Martín, J., Gasser, B., Rodriguez-y Baena, A., Toubal, T., and Fowler, S.: Dynamics of particle flux and carbon export in the northwestern Mediterranean Sea: a two decade time-series study at the DYFAMED site, Progress in Oceanography, 91, 461–481, 2011.

Morel, A.: Optical modeling of the upper ocean in relation to its biogenous matter content (case I waters), Journal of Geophysical Research: Oceans (1978–2012), 93, 10 749–10 768, 1988.

Moutin, T. and Prieur, L.: Influence of anticyclonic eddies on the Biogeochemistry from the Oligotrophic to the Ultraoligotrophic Mediterranean (BOUM cruise), Biogeosciences, 9, 3827–3855, 2012b.

Moutin, T. and Raimbault, P.: Primary production, carbon export and nutrients availability in Western and Eastern Mediterranean Sea in early summer 1996 (MINOS cruise), Journal of Marine Systems, 33, 273–288, 2002.

Moutin, T., Raimbault, P., and Poggiale, J.: Production primaire dans les eaux de surface de la Mediterranee occidentale. Calcul de la production journaliere, Comptes Rendus de l'Académie des Sciences-Series III-Sciences de la Vie, 322, 651–655, 1999.

Moutin, T., Thingstad, T. F., Van Wambeke, F., Marie, D., Slawyk, G., and Raimbault, P.: Does competition for nanomolar phosphate supply explain the predominance of the cyanobacterium Synechococcus?, Limnology and Oceanography, 47, 1562–1567, 2002.

Moutin, T., Karl, D. M., Duhamel, S., Rimmelin, P., Raimbault, P.and Van Mooy, B. A. S., and Claustre, H.: Phosphate availability and the ultimate control of new nitrogen input by nitrogen fixation in the tropical Pacific Ocean, Biogeosciences, 5, 95–109, 2008.

Moutin, T., Van Wambeke, F., and Prieur, L.: Introduction to the Biogeochemistry from the Oligotrophic to the Ultraoligotrophic Mediterranean (BOUM) experiment, Biogeosciences, 9, 3817–3825, 2012a.

Palmiéri, J.: Modélisation biogéochimique de la mer Méditerranée avec le modèle régional couplé NEMO-MED12/PISCES., Ph.D. thesis, Université de Versailles Saint-Quentin, France, 2014.

Palmiéri, J., Orr, J., Dutay, J., Béranger, K., Schneider, A., Beuvier, J., and Somot, S.: Simulated anthropogenic CO2 uptake and acidification of the Mediterranean Sea, Biogeosciences, 12, 781–802, 2015.

Palmiéri, J., Le Vu, B., Dutay, J., Bopp, L., Béranger, K., Beuvier, J., Somot, S., and Éthé, C.: Biogeochemical modelling of the Mediterranean Sea with PISCES MED-12 model., GMD, in prep.

Pasqueron de Fommervault, O., Migon, C., D'Ortenzio, F., Ribera d'Alcalà, M., and Coppola, L.: Temporal variability of nutrient concentrations in the northwestern Mediterranean sea (DYFAMED time-series station), Deep Sea Research Part I, 100, 1–12, 2015.

Paulmier, A., Kriest, I., and Oschlies, A.: Stoichiometries of remineralisation and denitrification in global biogeochemical ocean models, Biogeosciences (BG), 6, 923–935, 2009.

Prowe, A., Pahlow, M., Dutkiewicz, S., Follows, M., and Oschlies, A.: Top-down control of marine phytoplankton diversity in a global ecosystem model, Progress in Oceanography, 101, 1–13, 2012.

Pujo-Pay, M., Conan, P., Oriol, L., Cornet-Barthaux, V., Falco, C., Ghiglione, J., Goyet, C., Moutin, T., and Prieur, L.: Integrated survey of elemental stoichiometry (C, N, P) from the western to eastern Mediterranean Sea, Biogeosciences, 8, 883–899, 2011.

Santinelli, C., Nannicini, L., and Seritti, A.: DOC dynamics in the meso and bathypelagic layers of the Mediterranean Sea, Deep Sea Research Part II: Topical Studies in Oceanography, 57, 1446–1459, 2010.

Santinelli, C., D.A., H., and d'Alcala M., R.: Influence of stratification on marine dissolved organic carbon (DOC) dynamics : The Mediterranean Sea case, Progress in Oceanography, 119, 68–77, 2013.

Sarmiento, J. and Gruber, N.: Ocean biogeochemical dynamics, vol. 1015, Princeton University Press Princeton, 2006.

Sarmiento, J., Hughes, T., Stouffer, R., and Manabe, S.: Simulated response of the ocean carbon cycle to anthropogenic climate warming, Nature, 393, 245–249, 1998.

Schaap, D. and Lowry, R.: SeaDataNet–Pan-European infrastructure for marine and ocean data management: unified access to distributed data sets, International Journal of Digital Earth, 3, 50–69, 2010.

Siegenthaler, U. and Sarmiento, J.: Atmospheric carbon dioxide and the ocean, Nature, 365, 119–125, 1993.

Siokou-Frangou, I., Christaki, U., Mazzocchi, M., Montresor, M., Ribera d'Alcalà, M., Vaqué, D., and Zingone, A.: Plankton in the open Mediterranean Sea: a review, Biogeosciences, 7, 1543–1586, 2010.

Somot, S., Sevault, F., and Déqué, M.: Transient climate change scenario simulation of the Mediterranean Sea for the twenty-first century using a high-resolution ocean circulation model, Climate Dynamics, 27, 851–879, 2006.

Soto-Navarro, J., Somot, S., Sevault, F., Beuvier, J., Criado-Aldeanueva, F., García-Lafuente, J., and Béranger, K.: Evaluation of regional ocean circulation models for the Mediterranean Sea at the Strait of Gibraltar: volume transport and thermohaline properties of the outflow, Climate Dynamics, 44, 1277–1292, doi:10.1007/S00382-014-2179-4, 2014.

Sournia, A.: La production primaire planctonique en Méditerranée; essai de mise à jour, Cooperative Investigations in the Mediterranean, International Coordinator and Operational Unit; Étude en commun de la Méditerranée, Coordonnateur international et Unité opérationnelle, 1973.

Thingstad, T., , Hagström, A., and Rassoulzadegan, F.: Accumulation of degradable DOC in surface waters: Is it caused by a malfunctioning microbial loop?, Limnology and Oceanography, 42, 398–404, 1997.

Thingstad, T., Krom, M., Mantoura, R., Flaten, G., Groom, S., Herut, B., Kress, N., Law, C., Pasternak, A., Pitta, P., Psarra, S., Rassoulzadegan, F., Tanaka, T., Tselepides, A., Wassman, P., Woodward, E., Wexels, R., Zodiatis, G., and Zohary, T.: Nature of phosphorus limitation in the ultraoligotrophic eastern Mediterranean, Science, 309, 1068–1071, 2005.

Toggweiler, J., Gnanadesikan, A., Carson, S., Murnane, R., and Sarmiento, J.: Representation of the carbon cycle in box models and GCMs: 1. Solubility pump, Global biogeochemical cycles, 17, 2003.

Tugrul, S. and Besiktepe, S.: Nutrient exchange fluxes between the black sea and the Mediterranean through the turkish strait system (marmara sea, bosphorus and dardanelles), CIESM, 2007.

Uitz, J., Stramski, D., Gentili, B., D'Ortenzio, F., and Claustre, H.: Estimates of phytoplankton class-specific and total primary production in the Mediterranean Sea from satellite ocean color observations, Global Biogeochemical Cycles, 26, doi:10.1029/2011GB004055, 2012.

Vallina, S., Ward, B., Dutkiewicz, S., and Follows, M.: Maximal feeding with active prey-switching: A kill-the-winner functional response and its effect on global diversity and biogeography, Progress in Oceanography, 120, 93–109, 2014.

Van Den Broeck, N., Moutin, T., Rodier, M., and Le Bouteiller, A.: Seasonal variations of phosphate availability in the SW Pacific Ocean near New Caledonia, Mar. Ecol. Progress Ser., 268, 1–12, 2004.

Van Wambeke, F., Christaki, U., Giannakourou, A., Moutin, T., and Souvemerzoglou, K.: Longitudinal and vertical trends of bacterial limitation by phosphorus and carbon in the Mediterranean Sea, Microbial ecology, 43, 119–133, 2002.

Vichi, M., Pinardi, N., and Masina, S.: A generalized model of pelagic biogeochemistry for the global ocean ecosystem. Part I: Theory, Journal of Marine Systems, 64, 89–109, 2007.

Volpe, G., Santoleri, R., Vellucci, V., Ribera d'Alcala, M., Marullo, S., and d'Ortenzio, F.: The colour of the Mediterranean Sea: Global versus regional bio-optical algorithms evaluation and implication for satellite chlorophyll estimates, Remote Sensing of Environment, 107, 625–638, 2007.

Vörösmarty, C., Fekete, B., and Tucker, B.: Global river discharge database, RivDis, Tech. rep., 1996.

Wu, J., SUNDA, W., BOYLE, E., and Karl, D.: Phosphate depletion in the western North Atlantic Ocean, Sciences, 289, 759–762, 2000.

Zúñiga, D., Calafat, A., Sanchez-Vidal, A., Canals, M., Price, B., Heussner, S., and Miserocchi, S.: Particulate organic carbon budget in the open Algero-Balearic Basin (Western Mediterranean): Assessment from a one-year sediment trap experiment, Deep Sea Research Part I: Oceanographic Research Papers, 54, 1530–1548, 2007.

Appendix A: Model skill assessment

Due to the high complexity of the biogeochemical model and the scarcity of data, the assessment of the model's representativeness at the scale of the Mediterranean Sea is a complex task. This work, however, aims at performing comparisons on several modeled variables, at different time and space scales when in situ measurements were available. For reasons of brevity, model outputs hereafter have the prefix "m" while corresponding in situ or satellite observations have the prefix "o".

A1 Nutrients

A1.1 Basin scale spatial variability

Data collected during the BOUM cruise allow to appreciate the quality of the simulation during the stratified summer period. The comparison between mNO_3 and mPO_4 with the corresponding measured concentrations (i.e. oNO3 and oPO4) along the BOUM transect is done in Fig. 15 and Table 1. mNO_3 varies between 0.12 and 7.8 μmol l^{-1} in the Western basin, and between 0.36 and

5.7 μmol l^{-1} in the Eastern basin (Fig. **??**). mPO_4 varies between 0 and 0.34 μmol l^{-1} in the Western basin, and between 0 and 0.18 μmol l^{-1} in the Eastern basin (Fig. **??**). Corresponding ranges from BOUM data are wider (higher maxima) for both nitrate and phosphate, as summarized in Table 1.

When compared to in situ data, average mNO_3 [mPO_4 in brackets] is underestimated by 1.2 [0.04] μmol l^{-1} in the Western basin, and 0.4 [0.01] μmol l^{-1} in the Eastern basin. This can be attributed to an underestimation of initial nutrient stocks at depth. There are indeed significant differences between the nutrient concentrations in deep waters provided by the Medatlas climatology and by the BOUM measurements. As a consequence, and due to the stability of nutrient concentrations in deep water during the simulation, the same disparities can be observed between the model outputs and the BOUM cruise data.

In the surface layer (0-30 m), mNO_3 is less than 1 μmol l^{-1}, with a mean value of around 0.5 μmol l^{-1} for the whole basin, while mPO_4 is almost nil everywhere (< 0.01 μmol l^{-1}). These values are consistent with measured nutrient concentrations, which are low and close to their quantification limits of 0.05 μmol l^{-1} for both NO_3 and PO_4 (Fig. 15, Table 1) though the model tends to overestimate surface nitrate concentrations during periods of intense stratification. This may be related to an overestimation of nitrification processes, and/or an underestimation of detrital organic matter sinking. Nitrification is, indeed, a linear function with a fixed parameter and does not take into account potential dependancies of the process (e.g. Paulmier et al., 2009). Modeled nutrient concentrations increase with depth and remain at their maximum values from the bottom of the nutriclines to the bottom of the sea. Western basin average deep mNO_3 and mPO_4 are 7.7 and 0.34 μmol l^{-1}, respectively, and Eastern basin average values are 5.4 and 0.15 μmol l^{-1} respectively (Table 1). The modeled top nitracline is located at around 30 m depth along the entire BOUM transect. The top phosphacline depth ranges between 50 m and 120 m with a mean of about 80 m, except in the South Ionian Sea, where it ranges between 120 and 160 m (Fig. 15). In the Western basin, the top of the modeled nitracline is almost 25 m over the top nitracline derived from in situ data, and the gap increases eastward as the top nitracline derived from data gets deeper (Moutin and Prieur, 2012b). The modeled top phosphacline is also below the data-derived top phosphacline. The difference between model outputs and data can also be found in the slope of the nitracline at depths of between 150 m and 1000 m: this slope decreases with depth for the model, while it is quite constant for data. As a consequence, significant differences in nitrate concentration can be observed in the "intermediate" waters (between 250 and 1000 m) : model mean concentrations are underestimated by almost 3 μmol l^{-1} at 500 m in the Western basin, and respectively 1.5 μmol l^{-1} in the Ionian basin and 1.2 μmol l^{-1} in the Ionian and Levantine basins. In the Western basin, the same differences between model and data were found in the phosphate vertical profiles (Fig. 15, Table 1), resulting in a maximum difference of 0.15 μmol l^{-1} in phosphate concentrations. However, in the Eastern basin, modeled and in situ phosphate gradients are in better agreement than nitrate gradients, except that the phosphacline is less thick than in data. , leading to an underestimation of deep concentrations

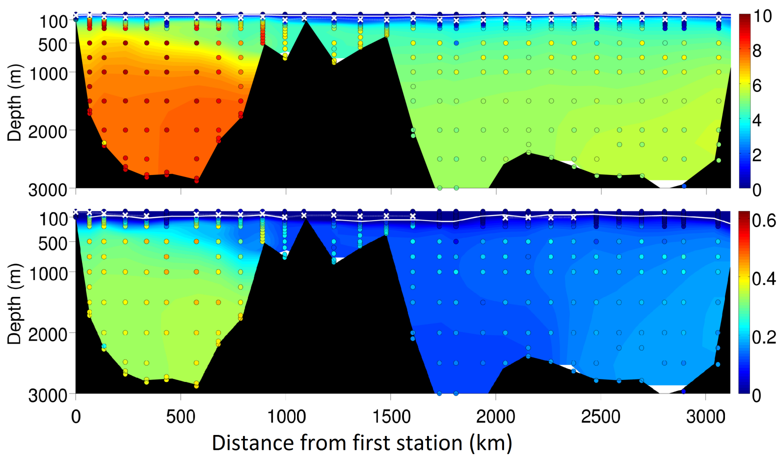

Figure 15. BOUM (top) NO_3 and (bottom) PO_4 (Pujo-Pay et al., 2011). The top figure is a detail of the lower figure. Model outputs are in shaded colors; in situ data are colored circles. Model outputs correspond to the daily outputs averaged over the BOUM cruise period. White crosses represent the data-derived depth of the top nitracline as defined in (Moutin and Prieur, 2012b). The white line indicates the top nitracline from model outputs.

by the model. Deep mNO_3 and mPO_4 decrease from west to east along a well-described gradient, which is in agreement with observations (Pujo-Pay et al., 2011). The mNO_3:mPO_4 ratio at 1500 m in the Western basin ranges between 21 and 24 and is very close to the measured ratio, which lies between 22 and 23. In the Eastern basin, the modeled ratio decreases eastward from 42 to 31, while the measured ratio ranges between 27 and 31. In addition, Finally, some discrepancies between model and observations are attributable to the hydrodynamic model (e.g. mislocation of the anti-cyclonic eddies, but this failure of the hydrodynamical model has only a local impact on modeled nutrients.

A1.2 Seasonal and vertical variabilities

At DyFaMed station, most of the spatial and temporal variabilities in nutrient concentrations are observed within the surface layer (see Fig. **??**, **??** and table 2). The surface evolutions of mNO_3 and mPO_4 at DyFaMed station are plotted in Fig. 16. In the upper layer (0-30 m), mNO_3 and mPO_4 exhibit a seasonal pattern, with values regularly lower than 0.5 μmol l^{-1} from May (March for mPO_4) to October, increasing thereafter to reach a maximum in January ranging from 3.2 to 4.2 (0.03 to 0.07 for mPO_4) μmol l^{-1} depending on the year. This is very similar to the evolution of observed NO_3 which is also below 0.5 μmol l^{-1} from May to October and reach a maximum ranging from 2 to 6.4 μmol l^{-1} in January-February. In summer, however, oNO_3 is often almost below the quantification limit while mNO_3 is never below 0.2 μmol l^{-1}. oPO_4 is below the quantification limit in almost every observation made above 30 m depth, except between January and March where oPO_4 can reach 0.15 μmol l^{-1}. These maxima are underestimated by the model, as mPO_4 never exceeds

Table 1. Mean over the BOUM cruise period of modeled (mNO_3, mPO_4) and measured (oNO_3, oPO_4) nutrients concentrations for different layers of the western and eastern basins. Root Mean Squared Difference (RMSD) between model outputs and observations have been calculated. Values in brackets are standard deviations, and BQL stands for Below the Quantification Limit (0.05 μmol l^{-1}).

		Model		Observations		RMSD	
		West	East	West	East	West	East
0-30 m	NO_3	0.4 [0.2]	0.6 [0.1]	BQL	BQL	0.44	0.67
	PO_4	0.02 [0]	0.002 [0]	BQL	BQL	0.020	0.0047
250-1500 m	NO_3	6.3 [1]	4.7 [0.4]	8.7 [1.1]	5.3 [1.4]	2.3	1.90
	PO_4	0.27 [0.1]	0.14 [0]	0.37 [0.1]	0.18 [0.1]	0.12	0.047
$>$ 1500 m	NO_3	7.7 [0.1]	5.4 [0.2]	8.9 [0.5]	5.0 [0.5]	1.2	0.33
	PO_4	0.34 [0]	0.15 [0]	0.38 [0]	0.16 [0]	0.049	0.032
Range	NO_3	[0 ; 7.8]	[0.36 ; 5.7]	[BQL ; 9.8]	[BQL ; 6.3]	2.1	1.7
	PO_4	[0 ; 0.34]	[0 ; 0.18]	[BQL ; 0.44]	[BQL ; 0.28]	0.11	0.042

0.07 μmol l^{-1} (close to the quantification limit). The differences between mPO_4 and oPO_4 at very low phosphate concentrations can be partly attributable to the lower reliability of measurements near the detection limit. For higher phosphate concentrations however, especially during the winter convection period, there is a clear deficit in the mPO4 which is not only due to the underestimated initial mPO4 concentration in deep waters (this has already been evidenced by the comparison with BOUM data, see section A1.1), but also potentially due to an underestimation of the MLD in winter).

In both model outputs and observations, the highest values of surface PO_4 and NO_3 correspond to the period of winter mixing (down to 100 m depth) in January-February. The 1 μmol l^{-1} isoline of nitrate (see Fig. **??**), which is a good indicator of the seasonal signal, has quite similar locations in the model and in data, lying at a maximum depth of around 40 m between March and October, and reaching the sea surface from November-December to March. For phosphate, the available observations show that the 0.1 μmol l^{-1} isoline reaches the surface during mixing, while the modeled isoline remains below 50 m depth.

Between 30 and 1000 m depth, observed and modeled NO_3 and PO_4 concentrations are consistent with each other though observations show higher mean values and larger ranges quite systematically (see Fig. 17 and 18 and table 2). The highest absolute differences along the water column are observed between 250 and 500 m depths for nitrate where mNO_3 is underestimated by 1.5 μmol l^{-1}, and between 30 and 100 m for phosphate where the mean mPO_4 is very low ($<$ 0.02 μmol l^{-1}) while oPO_4 equals 0.14 μmol l^{-1}. The same interpretation for this poor representation of the shape of the nutriclines (well marked in observations and much more diffuse in the model outputs) as the one provided for the comparison with BOUM profiles can be put forward to explain this model failure, namely underestimated deep nutrient concentrations and a lack of detrital particles that would have reached such water depths before being hydrolyzed. It must be reminded however that DyFaMed

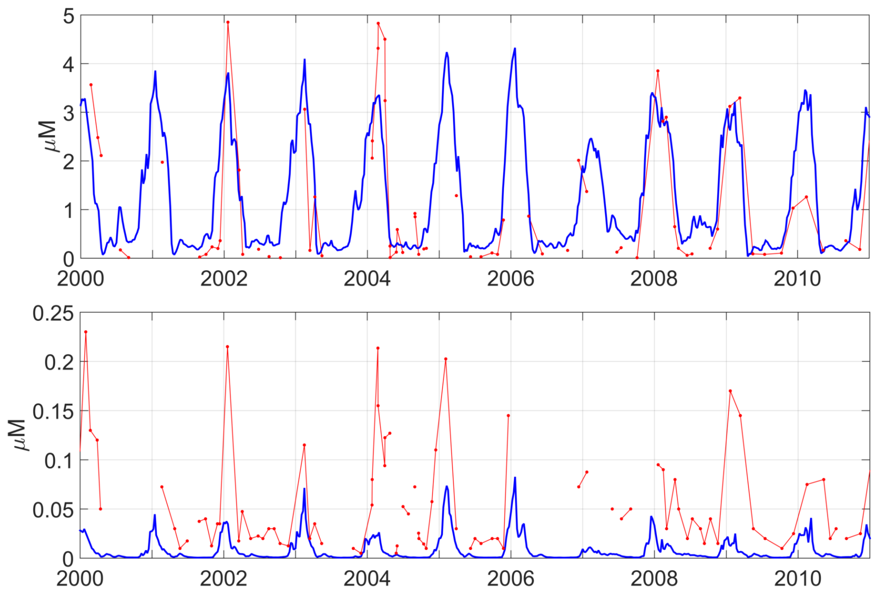

Figure 16. Time evolution of modeled (lines) and observed (dots) surface concentrations in nitrate and phosphate in μmol l^{-1} at the DyFaMed site.

observations are compared to a single grid point of the modeled domain which is submitted to variability due to hydrodynamical features. We evaluated potential impact of variability by calculating the RMSD between 8 neighbouring grid points and the single grid point chosen. The impact of spatial variaibility is weak on temporal means ($<$ 0.13 and 0.01 μmol l^{-1} for NO_3 and PO_4 respectively) and stay below 0.5 and 0.04 μmol l^{-1} for NO_3 and PO_4 respectively during the whole period, and therefore cannot fully explain the differences observed.

A2 Chlorophyll

A2.1 Basin scale variability

Four distinct periods (winter, spring, summer, and autumn) have been chosen to present the variability of both satellite (oCHL) and model-derived (mCHL) chlorophyll concentration climatologies Maps of the annual means of oCHL and mCHL over as well as their difference (i.e. oCHL-mCHL) over the 2002-2011 period are plotted in Fig. 19 . mCHL is calculated as the average concentration through the first 10 m of the water column. for the 2002-2011 period. The contrast in mCHL between the Western and Eastern basins is the highest during winter and spring, whereas it is marked throughout the year for oCHL. Excluding the coastal regions (depths lower than 190 m), median mCHL in the West [East in brackets] basin is equal to 0.21 [0.06], 0.66 [0.09], 0.10 [0.11] and 0.12 [0.12] μg l^{-1}, respectively for winter, spring, summer, and autumn, while the corresponding values for the median oCHL is equal to 0.27 [0.08], 0.24 [0.07], 0.05 [0.03] and 0.10 [0.05] μg l^{-1}.

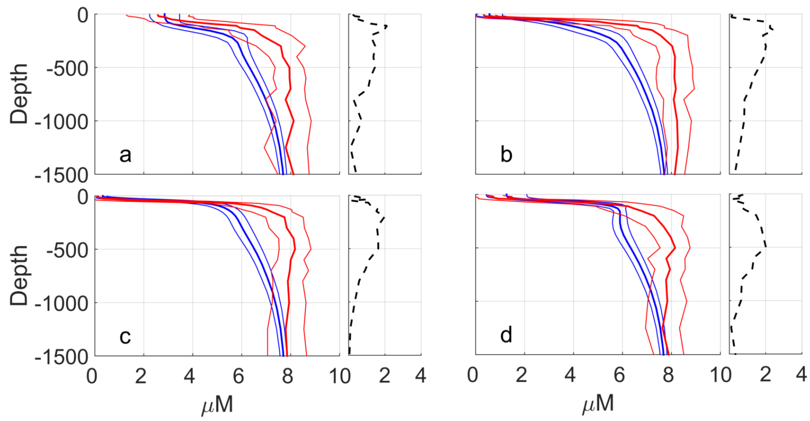

Figure 17. Seasonal climatologies over the 2000-2011 period of modeled (blue lines) and observed (red lines) concentrations in nitrate (μmol l^{-1}) at the DyFaMed site. (a) winter (Dec.-Feb.); (b) spring (Mar.-May); (c) summer (Jun.-Aug.); (d) autumn (Sept.-Nov.). Dotted lines on right panels represent the mean absolute bias between model and data.

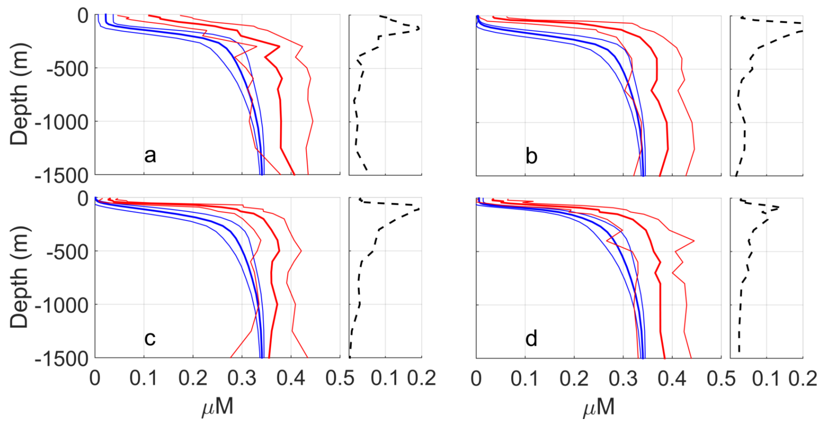

Figure 18. Seasonal climatologies of modeled (blue lines) and observed (red lines) concentrations in phosphate (μmol l^{-1}) at the DyFaMed site. (a) winter (Dec.-Feb.); (b) spring (Mar.-May); (c) summer (Jun.-Aug.); (d) autumn (Sept.-Nov.). Dotted lines on right panels represent the mean absolute bias between model and data.

At first, year-long high chlorophyll clusters can be seen in both oCHL and mCHL close to the main river mouths (the Nile, Rhone, Po, Ebro or Tiber), but only in oCHL in the Dardanelles Strait, along the western coast of the Adriatic Sea and in the Gulf of Gabes. For the Dardanelles Strait, the difference is likely due to a poor representation of the nutrients inputs at this boundary. For the Adriatic Sea, nutrient inputs from rivers are included in the model, but not the ones inferred by anthropic activities (domestic, industrial, agriculture), which may result in an underestimation of the nutrient inputs in this region, and therefore in an underestimation of the chlorophyll concentrations. Finally, the differences between mCHL and oCHL in the Gulf of Gabes is likely due to two main features:

Table 2. Mean over the 2000-2011 period of modeled (mNO_3, mPO_4) and measured (oNO_3, oPO_4) nutrients concentrations at the DyFaMed site for different layers. Root Mean Squared Difference (RMSD) between model outputs and observations have been calculated. Std stands for standart deviation. Spatial variability around the DyFaMed grid point is also assessed through the spatial standart deviation calculated using the 8 neighboor points (first column), and the value given is the highest deviation calculated during the 2000-2011 period.

			NO_3			
	Spatial Std	mNO_3 mean [range]	mNO_3 Std	oNO_3 mean [range]	oNO_3 Std	RMSD
0-30	0.22	1.3 [0.04-4.3]	1.1	1.0 [BQL-5.2]	1.4	1.1
30-100	0.32	3.0 [0.09 6.1]	1.3	3.8 [BQL-8.3]	2.2	1.8
100-250	0.25	5.1 [1.7-6.7]	1.0	7.0 [2.7-9.6]	1.4	1.4
250-500	0.13	6.2 [5.2-7.2]	0.39	8.1 [5.0-9.9]	0.8	2.0
1000-2000	0.03	7.6 [7.0-7.9]	0.21	8.0 [5.9-9.4]	0.75	0.81
			PO_4			
	Spatial Std	mPO_4 mean [range]	mPO_4 Std	oPO_4 mean [range]	oPO_4 Std	RMSD
0-30	0.001	0.008 [0-0.08]	0.12	1.0 [BQL-0.26]	0.06	0.07
30-100	0.02	0.02 [0-0.19]	0.03	0.14 [BQL-0.54]	0.10	0.16
100-250	0.03	0.15 [0.02-0.33]	0.09	0.29 [0.07-0.45]	0.07	0.17
250-500	0.001	0.29 [0.19-0.33]	0.03	0.35 [0.01-0.46]	0.05	0.08
1000-2000	0.001	0.34 [0.32-0.35]	0.01	0.37 [0.21-0.52]	0.05	0.05

first, this region is very shallow, which may produce less reliable satellite data. More importantly, the region of Gabes is characterized by an important industrial production of phosphate which effluents induce a strong enrichment in phosphate in this region, and this is not included in the model. Apart from these permanent features, the main differences between the model and satellite data are observed in the deep convection region of the Liguro-Provencal sub-basin (and extending up to the Ligurian Sea), along the Algerian coast, in the Alboran Sea, and in the south of the Eastern basin. seasonal chlorophyll patterns are compared, as follows. The three former are mostly attributable to failures of the hydrodynamic model: first, the fact that the contours of the modeled deep convection region are not the same as the measured ones have already been identified in the hydrodynamical simulation (Beuvier, 2011). Moreover, differences between measured and modeled MLD can also explain differences in the annual surface chlorophyll pattern as for example in the Ligurian Sea where an underestimation of the maximum mNO3 and mPO4 values, likely due to a deficit in the inputs of nutrients from deep waters during winter convection have been evidenced at DyFaMed station (see Fig. 16). The same is true for the Algerian current which is underestimated by the physical model. As a consequence, when the Atlantic waters arrive north of Algeria and Tunisia, they are more nutrient-depleted (and therefore less productive) than what is observed. Furthermore, the

Atlantic waters that flow along the coast are less dense and therefore strongly isolated from the rest of the water column and it seems that this property is excessively pronounced in the physical model. As a result, their nutrients content will be too rapidly consumed leading to underestimated primary production and Chl concentrations in this region. Finally, in the Alboran Sea, the high mesoscale activity is likely not fully captured by the hydrodynamical model. In the Eastern basin, the mCHL is overestimated nearly everywhere, and mostly in the southern part. This difference is however weak (less than 0.05 μg l^{-1}) and does not clearly appear in the climatology presented in Fig. 20. Overall, and apart from the hot spots already discussed, the maximum absolute error does not exceed 0.25 μg l^{-1} in the chlorophyll-rich regions of the Western basin (i.e. the deep convection region and the core of the eddies in the Alboran Sea) and 0.15(0.05) μg l^{-1} elsewhere in the Western(Eastern) basin. During winter (Fig. 19 a and e), high surface chlorophyll values are modeled and observed in the Western Mediterranean, particularly in the Alboran Sea where mCHL and oCHL values range between 1 and 2.4 and between 0.2 and 0.6 μg l^{-1}, respectively. The high oCHL in the Alboran Sea extends along the Algerian coast, a pattern not reproduced by the model. Elsewhere in the Western basin, oCHL is less patchy than mCHL since the model reaches high values in the deep convection area and low concentrations in the Tyrrhenian Sea that are not observed on the satellite map. On the other hand, the local minimum around 42°N 5 °E , where convection mixing is the most intense, is well-represented by the model. The Liguro-Provencal current associated with low concentrations is more clearly visible in mCHL than in oCHL (mCHL$<$ 0.1 μg l^{-1}). East of the Sicilian Strait, mCHL and oCHL values are mainly below 0.1 μg l^{-1} when the Adriatic Sea is not taken into account. In the open sea, the most visible pattern is the Rhodes Gyre with chlorophyll values above 0.2 μg l^{-1}. In the Adriatic Sea, mCHL and oCHL are both close to 0.2 μg l^{-1} (excluding the western coast) although mCHL is more patchy due to the presence of two structures with higher mCHL (from 0.3 to 0.6 μg l^{-1}).

During spring, the spatial pattern of oCHL (Fig. 19 b) is less homogeneous than in winter. The mCHL pattern (Fig. 19 f) is quite similar to the one modeled in winter, albeit with higher concentrations and sharper horizontal gradients. In the Western basin, mCHL values range between 0.3 and $>$ 3 μg l^{-1} and oCHL values range between 0.1 and $>$ 1 μg l^{-1}. In the Eastern basin, excluding the Adriatic Sea and the already mentioned permanent hot spots, chlorophyll concentration are low (around 0.1 μg l^{-1}), particularly in the south.

During summer, mCHL (Fig. 19 g) is quite homogeneous in the whole Mediterranean Basin and values are about 0.1 μg l^{-1} with the exception of some minimum values ($<$ 0.05 μg l^{-1}) in the area from the Algerian coast to the Balearic Islands and within the anti-cyclonic Alboran eddies, and some maximum values ($>$ 0.5 μg l^{-1}) in the north-western part of the Alboran Sea. oCHL values (Fig. 19c), are below mCHL values almost everywhere, at around 0.05 μg l^{-1} with the exception of in the North-Western Alboran Sea where they are above 0.5 μg l^{-1}. The chlorophyll decrease in the Algerian basin, the ending of the bloom in the Provencal sub-basin and the Rhodes Gyre, and the low concentrations in the Tyrrhenian Sea and Eastern basin are well represented by the model. However, the eastward gradient of oligotrophy is not clearly visible in the model.

During autumn, the situation is close to that in summer, with mean mCHL values of 0.1 μg l^{-1} (Fig. 19h). Local maxima (0.15 μg l^{-1}) are, however, discernable in the Provencal sub-basin, the Rhodes Gyre, the Eastern Corsica patch, and the region between Sardinia and Sicily. Other local maxima with higher concentrations (0.4 μg l^{-1}) are identified in the Alboran Sea, from the Gibraltar Strait to the cyclonic gyre located at 1°W. oCHL values are below 0.1 μg l^{-1} in the whole Mediterranean Basin with the exception of along the Algerian coast, the Alboran Sea, the Provencal sub-basin and the Adriatic Sea, where concentrations are higher but remain below 0.3 μg l^{-1} (Fig. 19d).

The mCHL variability is largely dominated by high values in the Alboran Sea as far as the Balearic Island (2°E) , following the pattern of the numerous mesoscale physical structures that are simulated in this area. However, according to satellite measurements, high productivity in the Alboran Sea is limited to the region west of 3°W. Along the Algerian coast, the high concentrations observed by satellite are not reproduced by the model.

In conclusion, the model is able to track the location and the seasonal dynamics of all the major productive areas detected by the satellite, namely the main river mouths, the North-Western Alboran Sea, the Rhodes Gyre and the Liguro-Provencal sub-basin, excluding the Gulf of Gabes, where the shallow depth combined with high coastal supplies that are not introduced into the model render correct representation of this area very difficult. In conclusion, though the aforementioned discrepancies between mCHL and oCHL, the model is able to track the location of: mCHL values modeled and satellite chlorophyll patterns show roughly the same main structures, namely i) most of the major productive areas (except the missing regions for which an explanation has already been put forward, ii) a well-marked Liguro-Provencal bloom, which is, nevertheless, more intense and more expanded in the model, iii) a clearly visible weakly productive northern current (NC), and iv) a patch with high chlorophyll concentrations in the Rhodes Gyre. Two patches with high core CHL values ($>$ 1.2 μg l^{-1}) are simulated in the Adriatic Sea and not observed in oCHL. On the contrary, the Adriatic Sea is highly productive in the model outputs, particularly within the two patches identified, but satellite observations do not support these findings. It is likely that a failure of the hydrodynamic model is responsible for this misrepresentation of the chlorophyll concentrations. During winter and spring (Fig. 19a,b,e,f), mCHL values generally tend to be higher than oCHL values and this is particularly true in the Western basin. Though all the aforementioned discrepancies, chlorophyll concentrations and spatial patterns are quite well reproduced by the model (Fig. 19), and this is also the case for some typical biogeochemical features of the Mediterranean Sea. For example, (i) the modeled spring bloom in the Provencal sub-basin is well separated from the coast by the weakly productive Ligurian Northern Current, (ii) the partition between Western and Eastern basins is visible eastward of the Sicilian Strait, (iii) the content of the Rhodes Gyre is higher than that of the Levantine.

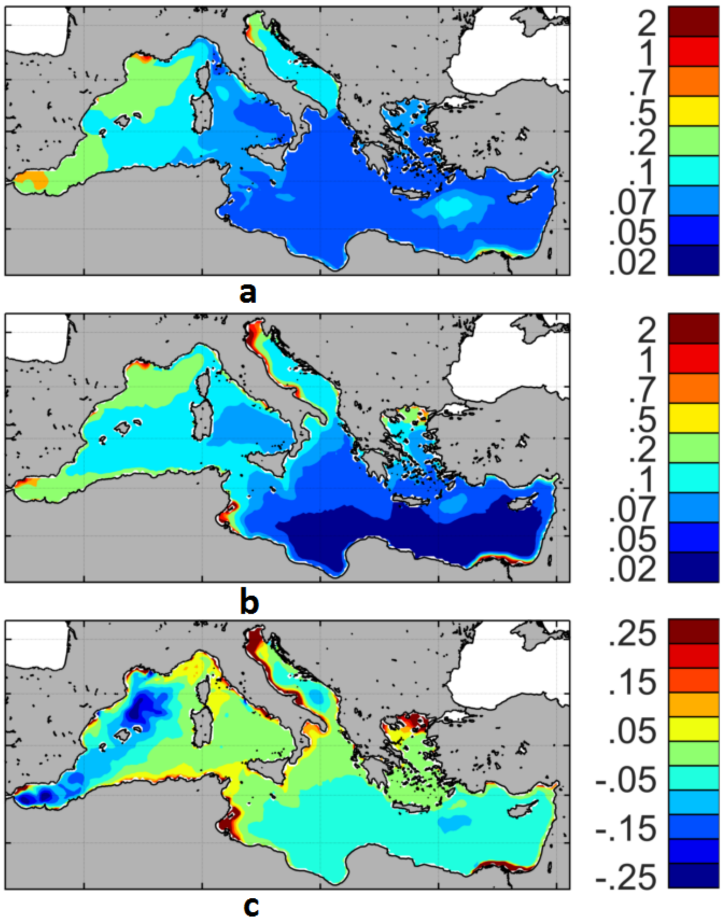

Figure 19. Maps of mean annual surface chlorophyll concentrations (μg l^{-1}) (a) from satellite (i.e. oCHL), (b) from model (i.e. mCHL), and (c) the difference oCHL - mCHL. Model chlorophyll (mCHL) is averaged over the first 10 m of the water column. Period used is 2002-2011 for both model outputs and satellite data.

The model values of the central Eastern basin are within the range of observations, with maximum values of below 0.3 μg l^{-1} (Fig. 19) in the open sea. However, minimum chlorophyll concentrations are obtained during spring by the model and this is in disagreement with observations. Models inter-comparison is beyond the scope of this paper, however comparisons with former simulations (Lazzari et al., 2012; Mattia et al., 2013) can give some informations. It is noteworthy that results from Mattia et al. (2013) showed a more important bias in the Eastern basin than in the Western basin, with higher annual concentrations compared to satellite measurements. The maximum of surface chlorophyll in the Eastern basin was simulated in winter (as for satellite chlorophyll) in Mattia et al. (2013). This is also the case in the simulation runned by Lazzari et al. (2012), however summer concentrations seemed to be underestimated in that case.

A2.2 Seasonal surface variability

Timing of chlorophyll seasonal variations is satisfactorily reproduced by the model when regarding the Provencal sub-basin, the Tyrrhenian Sea and the Rhodes Gyre (Fig. 19). To further study the seasonal variability of surface chorophyll, we used (for the satellite and model-derived chlorophyll concentrations) the metric ΔChl defined as follows :

$$\Delta Chl = \frac{\max(Chl_{\text{year}})}{\text{median}(Chl_{\text{year}})} \tag{A1}$$

Since chlorophyll time distribution does not follow a normal law, this indicator is likely more relevant than the mean and the standart deviation. Moreover, since applied to a climatology of chlorophyll outputs, extreme values have already been smoothed. High values of ΔChl can therefore be related to a strong seasonal variability, while low values, typically < 2, can be associated with a constant signal (Fig. 20).

For both model and satellite, the seasonal signal is particurarily important in the Liguro-Provencal sub-bassin ($\Delta Chl > 10$) and the Algerian Coast (ΔChl_{sat} about 8, ΔChl_{mod} above 10). ΔChl is broadly above 6 for model and 4 for satellite in the Western basin west of 9°W. In the Tyrrhenian Sea, ΔChl is close to zero for the model, except for the area along the Italian Coast, while ΔChl for satellite is above 3 with a maximum value around 6.

In the Eastern basin, model ΔChl is almost nil everywhere except in the Rhodes Gyre (> 10) and in the Adriatic Sea where two patches of values above 10 can be seen. This is consistent with oCHL values which are also low, except in the south Levantine basin (about 2), in the Rhodes Gyre (> 6) and in the Gulf of Gabes (> 6). In the Adriatic sea, a patch of values of ΔChl above 3 is visible in the South.

Using SeaWiFS and MODIS surface chlorophyll data from 1998 to 2010 and the statistical work from D'Ortenzio and Ribera d'Alcalà (2009), Lavigne et al. (2013) identified 9 different regions on the basis of the seasonality of the chlorophyll signal. These regions are consistent with the ones emerging from the present study. The North-West bloom region is associated with the region of the highest values of ΔChl_{mod} and ΔChl_{sat}. The Algerian region is characterized by relatively high ΔChl values, while the intermittent Rhodes Gyre region is identified as highly variable in the present study according to satellite data and model outputs. The distinction between the South and North Ionian basins in the bioregionalization, also visible satellite ΔChl is absent in the model ΔChl.

The comparison of modeled and observed time series (climatology over the 2000-2011 period) provides an additional information on the model ability to reproduce surface chlorophyll seasonal variations. Though the model values of the central Eastern basin are within the range of observations in the open sea (see Fig. 19), the highest discrepancy in the seasonal signal is observed in the oligotrophic region of the Levantine basin: However, the mCHL seasonal signal is in phase opposition with oCHL's one, and the minimum maximum mCHL chlorophyll concentrations are obtained

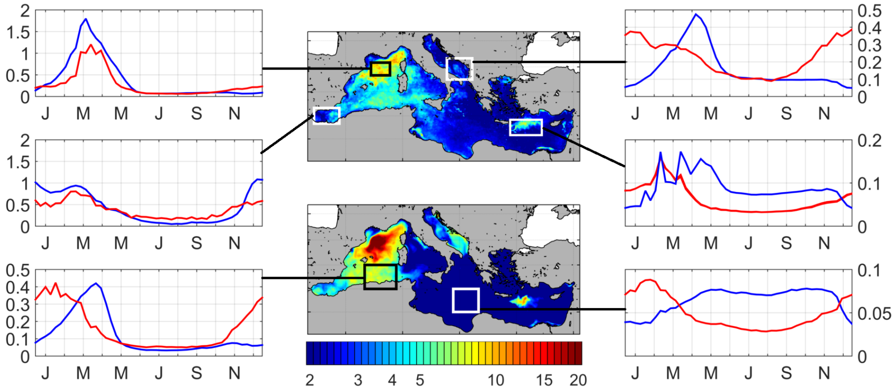

Figure 20. Maps of the ratio between annual maximum and annual median for satellite (top) and model (bottom) chlorophyll surface concentrations over the 2002-2011 period. A climatology of oCHL (red lines) and mCHL (blue lines) over the same period is also plotted for the most representative regions.

in summer-autumn spring against winter for oCHL. by the model and this is in disagreement with observations. Models intercomparison is beyond the scope of this paper, however comparisons with former simulations (Lazzari et al., 2012; Mattia et al., 2013) can give some informations. It is noteworthy that results from Mattia et al. (2013) showed a more important bias in the Eastern basin than in the Western basin, with higher annual concentrations compared to satellite measurements. However, the maximum of surface chlorophyll in the Eastern basin was simulated in winter (as for satellite chlorophyll) in Mattia et al. (2013). This is also the case in the simulation runned by Lazzari et al. (2012), however summer concentrations seemed to be underestimated in that case. This shortcoming can however be largely relativized by the fact that the mean surface chlorophyll in summer-autumn does not differ significantly from the satellite measurement. Furthermore, surface chlorophyll in the model is estimated as the mean over the first 10 m of the water column, and therefore includes part of the chlorophyll gradient towards the Deep Chlorophyll Maximum (DCM) which is shallower than the observed one in the Eastern basin during the stratification period (results not shown though the same bias is observed at the DyFaMed site, see Appendix A2.3). Finally, the summer functioning of the surface layer is well reproduced by the model : small phytoplankton are largely dominant and maintain their activity thanks to the microbial loop (Siokou-Frangou et al., 2010).

A shift in chlorophyll maximum can also be seen in the south of the Western basin, with an earlier and longer bloom in oCHL than in mCHL. This could be partly due to the already mentioned model tendency to exagerate the isolation of the surface Atlantic waters from the rest of the water column, thus delaying the input of nutrients from deep water through winter convection. Finally, in the Adriatic Sea, a delayed input of nutrients from deep waters combined with the presence of two eddies with high core mCHL values in winter and mostly in spring that are not observed on oCHL (the position of the two eddies can be seen on the primary production map in Fig. 22), likely explain the shift between oCHL and mCHL. Conversely, in regions associated with high nutrient inputs (Ligurian Sea, Alboran Sea) the temporal evolution of surface chlorophyll is reproduced by the model but concentrations are overestimated during the bloom in the deep convection region, likely due to a too intense winter mixing (Beuvier, 2011).

A2.3 Vertical and temporal variability

At the DyFaMed station, a strong seasonal variability in chlorophyll concentrations can be observed in both model outputs and in situ data (Marty et al., 2002; Marty and Chiavérini, 2010). Chlorophyll data (oCHL) and modeled ones (mCHL) are consistent with each other as shown in Fig. 21: they both show a bloom occurring in late February early March, after the period of maximum mixing (mid February in this area), characterized by high chlorophyll concentrations inside the mixing layer (down to 150 m depth). A second less intense and shallower bloom often follows in April, characterized by chlorophyll concentrations above 1.5 μg l^{-1} in both model outputs and observations. During summer, surface concentrations are at their lowest level with values of mChl and oChl often below 0.1 μg l^{-1}, while their maximum values are observed in early spring.

Following April, a Deep Chlorophyll Maximum DCM is visible in both observations and model, though it is shallower in the model and its intensity decreases more rapidly than in observations (see Fig. 21-top). the patch of high mChl (> 1.5 μg l^{-1}) deepens and the DCM settles down to ≈ 30 m depth with values about 0.2 μg l^{-1}, while oCHL DCM deepens to 50 m and its intensity slowly decreases down to concentrations around 1 μg l^{-1}.

During summer, surface concentrations are at their lowest level with values of mChl and oChl often below 0.1 μg l^{-1}. As the mixing layer depth gradually increases in autumn, mChl surface values first increase by dilution of the DCM (vertically integrated chlorophyll remains constant) and then decreases until the restart of primary production in early February. These results are consistent with the oCHL pattern. Surface chlorophyll is well reproduced by the model with a maximum observed in early spring and very low concentrations from June to October. Concerning the modeled DCM (Fig. 21-top), it is shallower than the one derived from observations. However, when looking at the two chlorophyll contributors of the model, it appears that the position of the DCM associated with large phytoplankton is close to the observed one. This means that the difference in the DCM depth is likely due to the underestimation of large phytoplankton concentrations at depth by the model during summer, that may be inferred by the already identified underestimation by the model of nutrient stocks in the intermediate layer (see section A1.1).

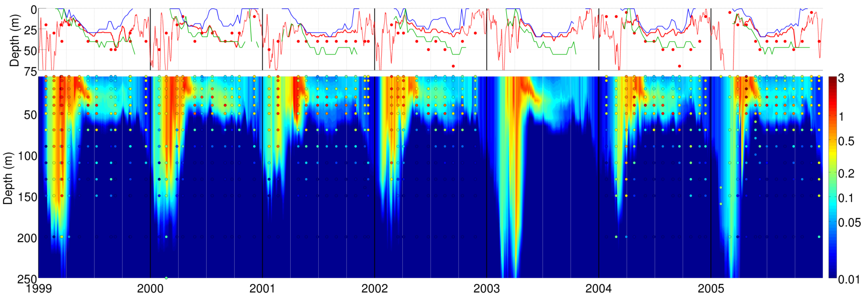

Figure 21. Time evolution of vertical concentrations of chlorophyll (μg l^{-1}) at the DyFaMed site, with model outputs in shaded colors and in situ data (Marty et al., 2008) in colored dots. On top, the depth of chlorophyll maximum is represented with red dots for in situ data and the red line for the model. When maximum is not obvious (see text), the line is dotted. Depths of maximum chlorophyll for small phytoplankton (blue) and large plankton (green) are also plotted.

A3 Primary production

In the following section, mIPP refers to the modeled integrated Gross Primary Production, i.e. to the total amount of inorganic carbon fixed by the two phytoplankton groups integrated over the water column. The equivalent for observations will be referred to as oIPP.

A3.1 Spatial variability

The mean annual mIPP of the whole basin over the 2000-2012 period equals 82 gC m^{-2} y^{-1}, which is in the range of published values (see Table 3). 98 (Lazzari et al., 2012), 80-90 (Sournia, 1973), 68 (Uitz et al., 2012), 136 (Bosc et al., 2004) or 156 (Antoine et al., 1995) using a coupled model, a climatology of ^{14}C measurements, and satellite-derived production in the last three references, respectively. In what follows, mIPP is compared to the oIPP derived from satellite data by Bosc et al. (2004) and Uitz et al. (2012).

In this table, Bosc et al. (2004) and Uitz et al. (2012) studies both show quite similar oIPP spatial distributions despite the two analyses having been conducted during different periods (1997-2001 for Bosc et al. (2004) and 1998-2007 for Uitz et al. (2012)). IPP calculated by Bosc et al. (2004) tend to overestimate observations, particularly in ultra-oligotrophic regions, but IPP from Uitz et al. (2012) does not show a trend of error. In the different regions defined in Bosc et al. (2004), mIPP is mostly within the range defined by the two studies. More importantly, the hierarchy in term of IPP between different regions is similar between model and satellite products. In the Western basin, the level of productivity of the different regions is the same, with the exception of the Algero-Provencal basin which is the less productive in both satellite products.

mIPP values in the Mediterranean Sea range between 35.4 and 270 gC m^{-2} y^{-1}, showing a strong spatial heterogeneity (see Fig. 22a). A gradient in mIPP is observed from west to east : the Western

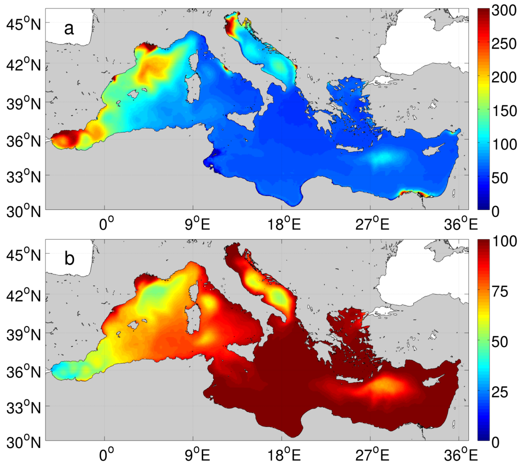

Figure 22. (a) Annual gross primary production calculated over the 2000-2012 period and integrated along the whole water column, in gC m^{-2} y^{-1}, (b) proportion of production due to small phytoplankton group, in % .

basin production is almost twice that of the Eastern basin, which is coherent with the dissimilarity in chlorophyll and nutrients already mentioned. This ratio is coherent with the o IPP derived from in situ measurements (Moutin and Raimbault, 2002), but higher than that found using the satellite or models (Uitz et al., 2012; Bosc et al., 2004; Lazzari et al., 2012).

Figure 22b shows that, except in the regions that benefit from permanent or episodic nutrients inputs from the deep sea (i.e. the deep convection region in the Liguro-Provencal sub-basin, eddies in the Alboran, Adriatic Seas and the Rhodes Gyre region), mIPP is mostly due to small phytoplankton in all the Mediterranean Basin. In the Eastern basin, the proportion of IPP due to small phytoplankton is close to 100% everywhere, except in the Levantine basin in the region of the Rhodes Gyre. These results are consistent with in situ studies (see the review in MERMEX-group (2011)).

A3.2 Seasonal variability

In addition to satellite data, in situ oIPP measured at the DyFaMed station between 1991 2002 and 1999 2006 (Marty and Chiavérini, 2002) (Marty et al., 2008) were used for comparison with mIPP (Fig. 23). Since in situ data and simulations cover different periods of time, we compared mean seasonal variations only. The model and observations show very similar patterns, with a maximum in March-April, and a slight decrease from July to December. Most daily measurements of primary production are within the interannual range of modeled values. The correlation between mIPP and oIPP is significative as suggested by the right panel in Fig. 23, and does not show any bias though the model fails in reproducing the highest oIPP values.

Table 3. Integrated gross primary production (mIPP in gC m^{-2} y^{-1}) for different regions of the Mediterranean Sea calculated by the model and derived from the following references: (a) Bosc et al. (2004), (b) Uitz et al. (2012) (c) Antoine et al. (1995), (d) Lazzari et al. (2012), and (e) Sournia (1973). References (a) to (c) refer to satellite data, (d) to a modeling study, and (e) to a climatology of ^{14}C measurements

Region	Model	(a)	(b)	(c)	(d)	(e)
Alboran Sea	222	150	230			
Gulf of Lion	182	97	194			
Balearic Sea	145	80	167			
Algero-Provencal basin	123	78	153			
Ligurian Sea	109	80	165			
Algerian basin	107	78	163			
Adriatic Sea	102	71	182			
Tyrrhenian Sea	66	67	137			
South Levantine basin	65	59	105			
North Levantine basin	63	60	106			
South Ionian Sea	60	61	115			
North Ionian Sea	55	63	126			
Mediterranean Basin	82	68	136	156	98	80-90

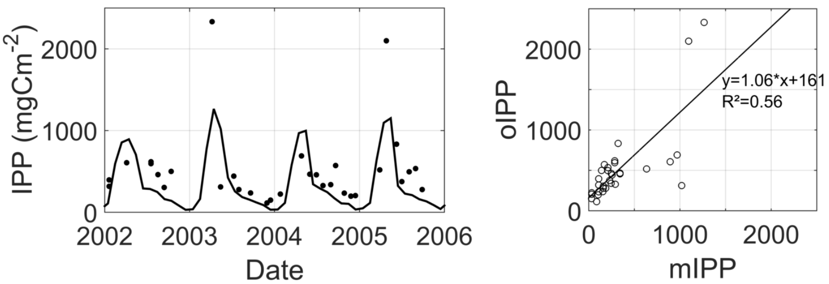

Figure 23. Time evolution of monthly integrated gross primary production (IPP) in mg C^{-2} d^{-1}. oIPP correspond to 0-100 m in situ measurements are values (depth integrated 0-100m) reproduced from (Marty and Chiavérini, 2002) extracted from the DyFaMed database (dots) and mIPP correspond to the 0-100 m IPP provided by the model during the same period (black line). oIPP were converted to daily gross primary production according to the Moutin et al. (1999) method. is the mean over the 2000-2012 period and grey are lines interannual maximum and minimum for every month.

A4 Dissolved organic carbon

Regular measurements of total DOC (i.e. including refractory (RDOC) and semi-refractory (SR-DOC) pools) performed at DyFaMed site (Avril, 2002) were used for comparison. Since the model only provides the labile and semi-labile DOC pools, the in situ DOC concentration measured in deep water (> 1000 m), which can be considered as refractory DOC, has been added to the model DOC output. Moreover, since our run does not cover the period of in situ data, we decided to work on a climatology of DOC vertical profiles: bi-monthly mean, maximal and minimal DOC values were calculated and compared (Fig. 24).

The climatology of DOC at DyFaMed proposed by Avril (2002) is divided into three periods. During spring, DOC stocks increase just after the bloom and DOC is related to the POC hydrolysis at depth. During summer, stratification isolates the surface layer where DOC accumulates due to the activity of small phytoplankton and to reduced bacterial activity. Then, during winter the water column is mixed.

At the DyFaMed grid point, mDOC stock is underestimated over the whole water column during winter. model outputs also Then, mDOC and oDOC show a DOC increase during spring (April-May), but only close to the surface for mDOC. Then, i In summer, the mDOC and oDOC values remain production rate high in the upper layers, is lower than in spring but still significant and limited to the upper layers. and finally decrease in autumn. Surface DOC stocks decrease (as of September) with mixing. If these seasonal variations are well reproduced by the model, high differences can however be seen between mDOC and oDOC. If we first focus on the 0-100 m layer, DOC concentrations and seasonal variations of both the model and observations are maximal at surface, but from spring to autumn, mDOC is higher than oDOC near the surface (roughly in the 0-50 m layer), and lower between 50 and 100 m depth, resulting in higher vertical DOC gradients in the model. The same discrepancy can also be evidenced (mostly in the Western basin) from the comparison between mDOC and oDOC during the BOUM cruise that took place in summer (Fig. 25).The overestimated near-surface DOC concentrations may be attributable to an excessive P-limitation in the model, likely due to too low phosphate deep concentrations (see also the Discussion section for the description of the DOC accumulation process under P depletion). The shallower and underestimated DCM as compared to the measured one (see section A2.3) may also explain part of the discrepancy since photosynthesis rates are underestimated. As a consequence, the excess of newly synthetized carbon through photosynthesis which fuels the DOC pool is likely underestimated in the region and even below the modeled DCM. A too easy access for bacteria to SLDOC resulting in an overcomsuption of DOC by nutrient-repleted bacteria is another possible explanation of this bias.

modeled mDOC variations concentrations are systematically lower than oDOC ones beyond 100 m depth. rapidly decrease with depth and they are lower than observations at 150 m depth. As a consequence, the mDOC vertical gradient is higher than the observed one, particularly in summer. DOC

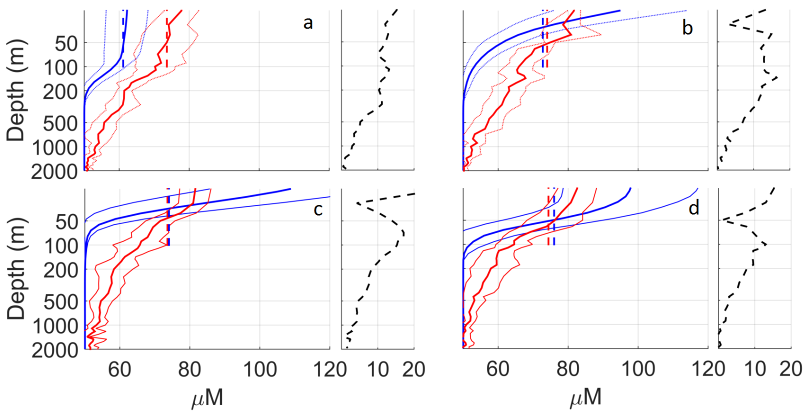

Figure 24. Vertical profiles of total DOC (μmol l^{-1}) at DyFaMed site. For each panel in situ data are plotted as dots, colors account for different time of sampling. mDOC are weekly averaged outputs. Black Blue and red lines respectively refer to modeled (mDOC) and measured (oDOC) DOC. Thick lines represent the mean of DOC over the period, while thin lines represent the standart deviation for each depth. oDOC and mDOC respectively cover the 1991-1993 (Avril, 2002) and the 2000-2012 period. The dotted lines in the right panels represent the mean absolute bias between oDOC and mDOC.

stocks variations are higher in the model : integrated DOC within the first 100 m ranges between 5.5 and 9.4 mol m^{-2} for the model, and between 7.2 and 8.7 mol m^{-2} for in situ data.

The latter could also partly explain the systematically underestimated mDOC concentrations below 100 m depth. Again, this model failure is also observed in during the BOUM cruise (Fig. 25). However, the comparison between oDOC and mDOC requires the addition of an unknown DOC component, namely the semi-refractory and the refractory pools, to the mDOC value. It is indeed generally assumed that both these pools are constant across the water column and that they correspond to the deep DOC concentration (i.e. 40 μM at DyFaMed station), but this is a clear source of bias, especially below 100 m depth where the SRDOC concentrations is significative and may vary as suggested in Santinelli et al. (2010).

The fact that the modeled 0-100 m integrated stocks are quite similar to the measured ones (though the slight underestimation in the Eastern basin during the BOUM cruise since DOC accumulation has not yet reached its maximum value in summer) is however an essential point as regards the DOC export at 100 m.

Finally, the Taylor diagram presented in Fig. 26 summerize the numerous comparisons between model outputs and DyFaMed station observations that have been undertaken in the present study.

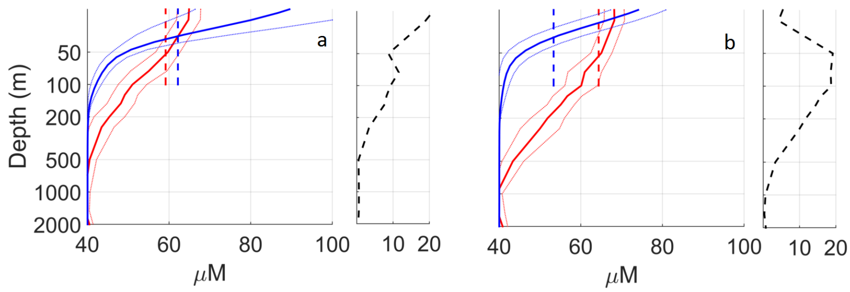

Figure 25. Vertical profiles of total DOC (μmol l^{-1}) during the BOUM cruise. mDOC are weekly averaged outputs over the whole BOUM section. Blue and red lines respectively refer to modeled (mDOC) and measured (oDOC) DOC. Thick lines represent the mean of DOC over the period, while thin lines represent the standart deviation for each depth. The dotted lines in the right panels represent the mean absolute bias between oDOC and mDOC.

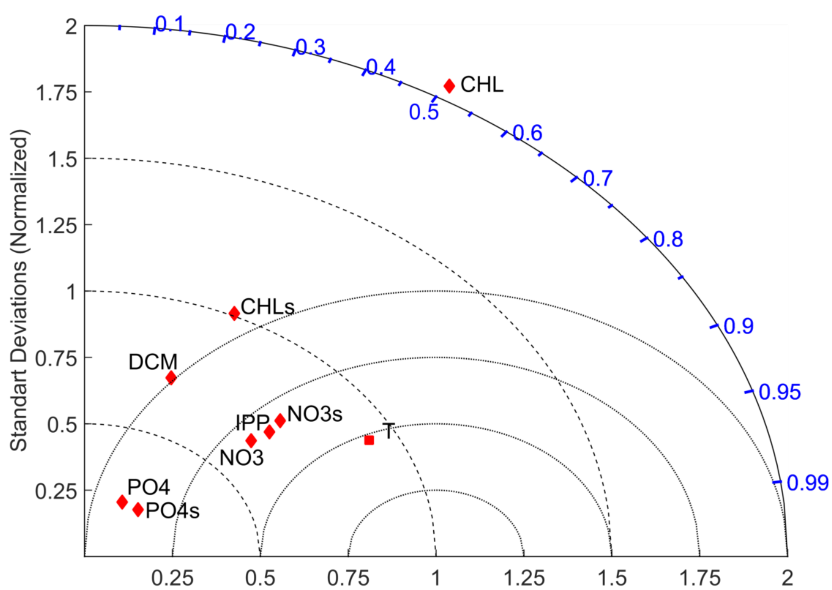

Figure 26. Taylor diagramm of simulated and observed variables in the 0-100 m layer. Model outputs and in-situ data are taken at the same depth and time. PO4s, NO3s ans CHLs are surface concentrations of phosphate, nitrate and chlorophyll respectively. T refers to temperature. Chlorophyll concentrationg are log-transformed.